NCMRWF

NCMR/TR/5/2011

TECHNICAL REPORT

Implementation of Upgraded Global Forecasting Systems (T382L64 and T574L64) at NCMRWF

V.S. Prasad, Saji Mohandas, Munmun Das Gupta, E.N. Rajagopal and Surya Kanti Dutta

May 2011

National Centre for Medium Range Weather Forecasting
Ministry of Earth Sciences
A-50, Sector 62, NOIDA – 201307, INDIA

Implementation of Upgraded Global Forecasting Systems (T382L64 and T574L64) at NCMRWF

V.S. Prasad, Saji Mohandas, Munmun Das Gupta, E.N. Rajagopal and Surya Kanti Dutta

May 2011

National Centre for Medium Range Weather Forecasting
Ministry of Earth Sciences
A-50, Sector 62, NOIDA – 201307, INDIA

Summary

This report summarizes the up-gradation of the NCMRWF Global Forecasting Systems (GFS) from T254L64 to the latest Global Data Assimilation and Forecasting (GDAF) system at T382L64 and T574L64 resolutions on IBM P6.

T382L64 system was implemented in May, 2010 and later a parallel upgraded system was also implemented at a resolution of T574L64 in November, 2010 with all the latest developments in the data decoding, assimilation, model and pre/post processing. A large number of satellite and non-conventional data are being assimilated in the new GDAF system. The T574L64 contains all the model developments in July, 2010 version of NCEP GFS, including a number of modifications in the model physics parameterisations effected through the namelist options. T382L64 system was run and tested for Monsoon-2010 along with old T254L64 systems though there are only minor modifications in the model physics for the T382L64 model, which is more close to T254L64 physics, but with major modifications in data input and assimilation. The new models are run in hybrid levels and with a forecast lead period of 10 days whereas T254L64 is having sigma levels with a forecast lead period of 7 days. A number of new diagnostics are generated in the new post processing systems which are listed in detail. The implementation was conducted keeping in mind with an emphasis on the easy portability of the GFS file structure between the user accounts and a central model source code repository in future up-gradations. All the three systems were run in parallel for a couple of months after Monsoon 2010 and an inter-comparison were also carried out during the winter season of December 2010- February 2011. The impact of the improvement in data assimilation and model is clearly evident from the case studies and the model verification statistics with T382L64 and T574L64 scoring over T254L64 system.

Contents

1. Introduction

National Center for Medium Range Weather Forecasting (NCMRWF) is working on research and development of numerical weather prediction models in India. Since 1994, it is carrying out near real time runs of Global Data Assimilation and Forecasting (GDAF) system based on National Centers for Environmental Prediction's (NCEP) Global Forecasting System (GFS). The initial system was implemented at a horizontal resolution of T80 with 18 vertical layers (T80L18) on CRAY supercomputer (see Table 1 for the history of computing systems used at NCMWF and Table 2 for the global models). Many changes were carried out to the same system from time-to-time and also ported on different computer platforms and continued to be the backbone of NCMRWF till end of 2006. Many applications such as Location Specific forecast for agriculture, wind energy, special event forecasts, and forecast for adventure sports etc were developed based on this T80L18 system.

From 1st January 2007, T80L18 GDAF system was replaced with newer updated version based on that day operational version of NCEP GFS system (Hereafter the terms GDAF and GFS may be used interchangingly). This system was implemented mainly on PARAM and CRAY-X1E systems at a reduced horizontal resolution of T254 from T382 due to limitation of computing power. This new T254L64 system contains all the changes that NCEP implemented in its GFS system during the period 1995- 2006 (See Rajagopal et. al 2007 for the description of the system). Apart from the changes in model, major changes in the system are the assimilation of direct satellite radiances and the data handling system. In the older T80 system input data is packed in a format called PREPQM and in the present system it is replaced with NCEP-BUFR format.

In T80L18 GDAF system, the data was decoded using ECMWF decoders and then packed into PREPQM format. Thus data pre-processing was unique at NCMRWF and was different from NCEP GFS. NCMRWF maintained this uniqueness till the implementation of T254L64 system. This became major bottle neck in implementing updated version of GFS and thus Rajagopal et al. (2007) implemented ‘NCEP decoder based’ data pre-processing system on PARAM computing system so that the data can be packed into NCEP-BUFR format easily. Hence, in Rajagopal et al. (2007) GFS implementation, data pre-processing, post processing and visualisation are on PARAM and assimilation-forecasting system is on CRAY-X1E. This dual-platform approach was adopted to

avoid some practical problems and to make the implementation simple.

Table 1: High Performance Computing (HPC) used at NCMRWF.

S.No.	HPC (with performance)	Period
1	Cray –XMP (4 Mflops)	1988-1993
2	Cray – YMP (16 Mflops)	1993-1998
3	Dec-Alpha (9.6 Gflops)	1999-2011
4	Cray SV1 (28.8 Gflops)	2001-2006
4	PARAM (500 Gflops)	2006-2011
5	Cray -X1E (1.1 Tflops)	2006-2011
6	IBM- Power 6 (24 Tflops)	2010 onwards

Table 2: Various global Models tested at NCMRWF.

Model	Year	Forecast Range
R40L18	1989	5 days
T80L18	1992	5 days
T170L28	2004	5 days
T170L42	2006	5 days
T254L64	2007	7 days
T382L64	2010	10 days
T574L64	2010	10 days

In the year 2010, NCMRWF acquired new IBM-P6 HPC and this report deals with implementation of end-to-end GFS system on new HPC. While designing the implementation, the directory structure is re-organised so that concept of "Repository" can be introduced. This will easily enable in implementing the branches of this model at other institutions to carry out joint development work. It will also help in maintaining different versions of the system all the times. This new directory structure is discussed in Section 2. The user-friendly organization of GFS system enables one to specify the model resolutions through the namelists. Thus a number of horizontal resolutions were tested namely, T382L64, T574L64 etc. The sections (3-5) describe the major updates of GFS analysis, forecast and post-processing systems from the T254L64 system. T382L64 was implemented from May, 2010 onwards on experimental mode. Section 6 discusses the

comparative performance of T254L64 and T382L64 models and some case studies. Section 7 deals with the distinction between the T382L64 and T574L64 implementations and the up-gradation issues and Section 8 with the inter-comparison of the three models followed by the section on summary.

2. Porting on IBM

While porting on the IBM system, a directory structure as shown in the figure 1 is designed so that branches of this system can be made easily in every user home directory with all GFS related subdirectories kept under 'gfs' home directory in user main home directory. The '$HOME/gfs' directory should contain at least two main subdirectories, 'nwprod' and 'nwdata'. 'nwprod' is the main production area containing source codes and anything and everything required to run or process the various systems related to GFS. It does not grow in size and should not be altered by the end users after the setting up of the model, except the minimum changes required for the job submission. All permanent files and directories such as those containing source codes, fixed files, libraries, job files, scripts, utilities etc. are kept in 'nwprod' directory in the respective subdirectories. An important directive for the model developers and application developers is that they should place any additional user applications (source codes, scripts, utilities etc.) and necessary fixed data sets in 'nwprod' area in the respective subdirectories. Also it is very important not to congest the 'nwprod' area by writing the output data, log files or any new derived data which are being periodically dumped, so that the size of 'nwprod' area is kept the minimum and permanent as possible. This helps in the maintainance and periodic up-gradation of source code and migration of GFS resources.

The directory 'nwdata' is the single repository of all important time-varying input and output data files required for and generated by the GFS modelling system. Thus to start with, the necessary observation datasets for a particular application for a particular time period of interest need to be copied to $HOME/gfs/nwdata tree branch in the corresponding locations so that the scripts and source codes in the 'nwprod' directory need minimum alteration or editing. Thus day-to-day bufr-tank files (data files), assimilation cycle input and output files, forecast output files, post-processed files etc. are organised in date-wise subdirectories within 'nwdata' directory with the names 'bufr_tank', 'gdas', 'fcst' and 'post' respectively. This is a directory which grows in size with time and the data files contained in it are the most important basic data sets which need to be preserved or

periodically archived on secondary storage media.

Apart from the two directories mentioned in the previous paragraphs, there can be any number of directories inside gfs home area, which are related to the GFS output processing and tailored user output datasets. Two more optional directories which are related to the running of GFS system are 'nwwork' and 'nwplot'. Directory 'nwwork' should be restricted to unimportant and miscellaneous intermediate files, logfiles and temporary working directories which are not necessary to be archived and can be removed periodically. The work areas related to the different components of the GFS system can be aptly named as gdas, fcst, post, plot etc.. Similarly, 'nwplot' is reserved for keeping various graphical outputs generated by the post-processing and visualisation tools. All the output data files and graphics should be kept in subdirectories with the names containing the corresponding date stamps. For example, the datasets are kept in the respective paths with the top directory named as 'gdas.YYYYMMDD'. In this fashion the permanent files are maintained in one directory (nwprod), and are kept away from the daily run outputs and the repository of this directory can maintain different versions.

Fig. 1 Diagram showing the base directory structure of gfs

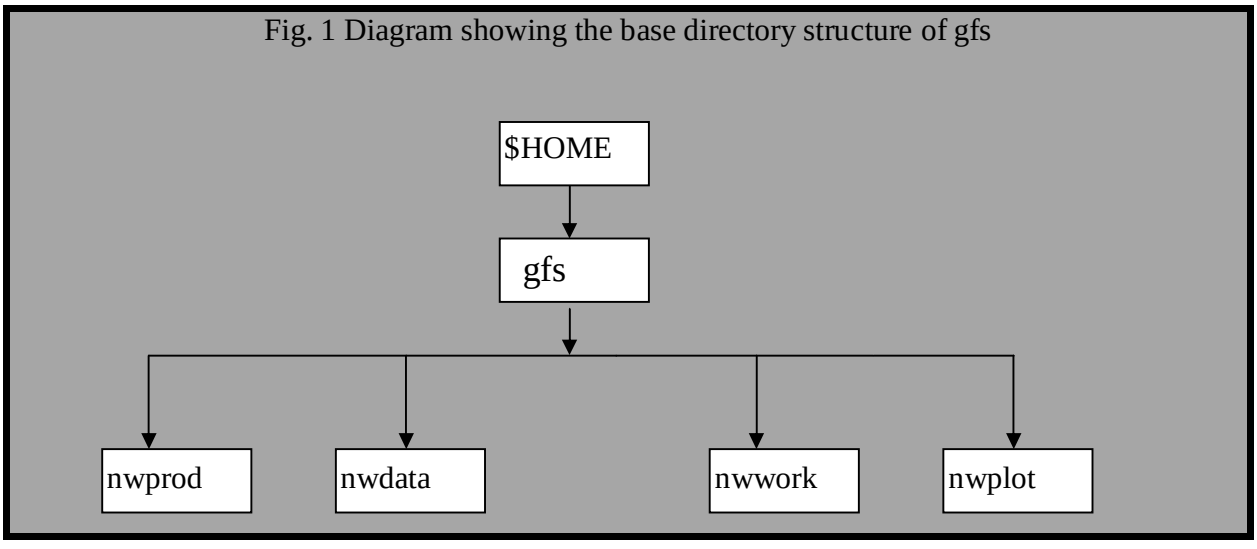

FORTRAN programs of the various components for the global analysis-forecast system are located in ${HOME}/gfs/nwprod/sorc in the directories listed below:

global_angupdate.fd
global_sig_igen.fd

global_chg_igen.fd
global_sigavg.fd
global_chgres.fd
global_sighdr.fd
global_cycle.fd
global_sigzvd.fd
global_fcst.fd
global_gsi.fd
global_postevents.fd
global_postgp.fd
global_satcount.fd
global_sfchdr.fd

FORTRAN libraries used by GFS analysis and forecast model are located in ${HOME}/gfs/nwprod /lib and are listed below:

liblandsfcutil_d.a
libcrtm_gfsgsi.a
libcrtm2.a
libbufr_4_64.a
libbufr_8_64.a
libbufr_d_64.a
libbufr_4_32.a
libbufr_s_64.a
libip_4.a
libip_8.a
libip_d.a
libsigio_4.a
libbacio_8.a
libbacio_4.a
libsp_4.a
libsp_8.a
libsp_d.a
libsfcio_4.a
libesmf_3_1_0rp2.a
libw3_4.a
libw3_8.a
libw3_d.a

The source codes of the FORTRAN libraries used by the GFS are located in ${HOME}/gfs/nwprod /lib/sorc in the directories listed below:

bacio
bufr
crex
crtm

decod_ut
esmf
ip
irsse
landsfcutil
sfcio
sigio
sp
w3

The source codes of decoders, data dump, and prepbufr are also kept in different subdirectories in ${HOME}/gfs/nwprod/sorc.

3. Analysis Scheme

In Rajagopal et al. (2007), the global analysis scheme used is Spectral Statistical Interpolation (SSI). However from January 2008, SSI system has been replaced with new Grid-point Statistical Interpolation (GSI). This GSI scheme was developed at the Environmental Modeling Center (EMC) at NCEP as part of an effort to create a more unified, robust, and efficient analysis scheme. The key aspect of the GSI is that it formulates the analysis in model grid space, which allows for more flexibility in the application of the background error covariances and makes it straightforward for a single analysis system to be used across a broad range of applications, including both global and regional modeling systems and domains. In the new GSI system many new features are included; like changes to the observation selection, quality control, minimization algorithm, dynamic balance constraint, and assimilation of new observation types.

GSI analysis scheme (Wu et al., 2002) is the evolutionary combination of the SSI analysis system and the regional ETA 3D-VAR. It replaces spectral definition for background errors with grid point (physical space) version based on recursive filters. This global 3DVAR in physical space is as effective as 3DVAR in spectral space with latitude-dependent structure functions and other error statistics. Diagonal background error covariance in spectral space (in SSI) allows little control over the spatial variation of the error statistics as the structure function is limited to being geographically homogeneous and isotropic about its center (Parrish and

Derber, 1992; Courtier et al., 1998). GSI allows greater flexibility in terms of inhomogeneity and anisotropy for background error statistics (Wu et al. 2002). Thus major improvement of GSI over SSI analysis scheme is its latitude-dependent structure functions and has more appropriate background errors in the tropics. The background error covariances are isotropic and homogeneous in the zonal direction. Thus results form initial experiments reported that GSI, had a small impact on extra-tropics but it had shown consistent positive impact in tropics (Wu et al 2002).

The frame work for the development of GSI has been taken from SSI - a three dimensional variational data assimilation (3DVAR) - and hence estimates initial state of the atmosphere achieved by minimising the cost function:

$$J(x) = \tfrac{1}{2} (z - h(x))^T R^{-1} (z - h(x)) + \tfrac{1}{2} (x - xb)^T B^{-1} (x - xb) \quad -- 1$$

Here, vector x represents the analyzed fields, z observations, $h(x)$ is the 'forward operator' expressing the observed variables in terms of the analyzed fields, and xb is the background field. Matrices, R and B represent error covariances, the first one of the measurements and of the forward operator, and the second of the background field. The improvement balance between the variables has been achieved through the inclusion of a tangent-linear normal-mode constraint (TLNMC), but not through additional generic constraint, Jc.

The original implementation 3DVAR is a time intermittent system, there is no place for inclusion of the temporal distribution of observations, and the difference between the observations and the background is assumed constant over the analysis time interval. With an explosive increase of the number of non-conventional datasets, such as satellite radiances (e.g., Derber and Wu 1998; Okamoto and Derber 2006; Le Marshall et al. 2001) or Global Positioning System (GPS) radio occultations (e.g., Cucurull et al. 2007), the need for including temporal distribution of data available for assimilation, even within a 3DVAR data assimilation approach, is felt. In GSI, this is achieved by modifying the first term in the formulation of the objective function, Jo, by taking account of observation time:

$$Jo(x) = \tfrac{1}{2} (z - h(x + (\partial x/\partial t)F\,\Delta t))^{T} R^{-1} (z - h(x + (\partial x/\partial t)F\,\Delta t) \quad \text{--- 2}$$

Here, **t** is the time increment of the observation **z** relative to the analysis time, $(\partial x/\partial t)F$ are filtered time tendencies of the analysis at the points surrounding this observation. Consequently, while stepping through the preconditioned conjugate gradient algorithm, in the calculations of the gradient of the objective function, search direction and the step size, the effect of the filtered time tendencies is consistently taken into account.

A simplistic parameterization of the planetary boundary layer (PBL) is added to the definition of time tendencies. It is based on the Janji´c (1990) implementation of Mellor and Yamada (1974) 2.0 closure scheme. This PBL parameterization is sufficiently simple to allow relatively quick calculation of a tangent linear version and its adjoint, but still complex enough to describe elements of turbulent mixing as a function of both thermal and dynamical conditions of the atmosphere. During development of the tangent linear version of the parameterization, additional simplifications were made. The most notable one was the 'assumption of the K-theory', which consisted of neglecting the vertical derivatives of turbulent coefficients (Dusanka Zupanski, personal communications). This approximation reduced the nonlinearity of the parameterization, and resulted in more realistic account of the PBL within the GSI analysis.

The GSI is included in the NCMRWF GDAF system and assimilations runs are carried out in six hour time intermittent method. In this, a new estimate of the atmospheric state (analysis) is required every 6 h to initialize a new 9-h global model forecast. Although the background used for each analysis is the previous 6-h forecast, a 9-h forecast is necessary to allow for time interpolation of asynoptic observations that fall within the 6-h analysis time window (i.e., time interpolation of the background is done between the 3-, 6-, and 9-h forecasts that covers the 6-h data window centered on the analysis time). The analyses are then used as the initial conditions for subsequent forecasts and the cycle continues. The complete details of the GSI system can be found in Kleist et al. (2009) and the results of pre-implementation test carried out at NCMRWF can be found in Rajagopal et al. (2008).

The meteorological observations from all over the globe are received at Regional Telecommunication Hub (RTH), New Delhi through Global Telecommunication System (GTS) and the same is made available to NCMRWF through a dedicated link. Most of these GTS bulletins are decoded from there native format and encoded into NCEP BUFR format using various decoders and stored in Tank files. Satellite radiances as shown in Table 3 are downloaded from NOAA/NESDIS and NCEP data servers.

GDAF system accesses the observational data base at a set time each day (i.e. the data cut-off time, presently set as 6hour) four times a day. Observations of similar type as mentioned in Table 3 and 4 are dumped into individual BUFR files, in which duplicate reports are removed and upper-air report parts are merged. The observation types that are mentioned in Table 3 are referred as conventional observations and they are all merged into single file called "prepbufr". This step involves the execution of series of programs designed to pack all conventional observations from there individual dump files along with their respective observational errors, and background (first guess) interpolated to each data location. During packing, various quality checks are also performed and with all these information, the data is encoded into the PREPBUFR files. Quality control of satellite radiance data is performed in analysis scheme itself.

The analysis procedure is performed as series of iterative problems. There are three main external iterations, which take care of the non-linearities in the objective function Jo. Each of the external iteration comprises of several operations for generating the analysis. The difference between the current solution and the observation is found by interpolating the 3, 6, and 9 hour forecast (or the current solution after the first external iteration) of the model variables to the observation time. The model variables are then transformed to the pseudo-observation variables, for example radiances, total perceptible water, bending angle etc. For satellite-measured radiances, the model profiles of temperature, moisture, and ozone along with various surface parameters are transformed into pseudo-radiances by using a Fast Radiative Transfer Model (FRTM) called, Community Radiative Transfer Model (CRTM). These pseudo-observations are then compared to the actual observations after applying quality control and bias corrections etc. and an observational increment (innovation) is created. The final observation is generated by

modifying the background with the help of observational increments. Table 5 and the following three figures (2-4) give an idea of the quantum of observations assimilated on a particular day along with the data coverage of GPSRO, Satellite radiance and AMV datasets respectively.

Table 3: Conventional data sets that are assimilated in the GSI, typical example on 23rd, Dec 2010 00z cycle.

S.No	**Observation Type**	**Observation Subtype**	**Total obs.**
1	Upper air Soundings	TMPLND(632),TMPSHP(2),TMPDRP(0), TMPMOB(0), PILOT(102), Profiler(7)	743
2	Surface Observation	Lndsyn(10688),ship(1813),buoy(1105), Metar(12029), mobile/AWS(5121)	40666
3.	Aircraft	Airep(812), Amdar(17746), Acars(41606)	60164
4	Satellite winds	GOES-11(5081), GOES-13(260184), MSG(28455), Meteosat(35384), GMS/MTSAT (21036)	116140

Table 4: Satellite data sets that are assimilated in the GSI .

S. No	**Sensor**	**Data type**	**Satellies**
1	AMSU-A	Radiance	Aqua, Metop-A, N15, N18, N19
2	AMSU-B	Radiance	N15, N16, N17
3.	MHS	Radiance	Metop-A, N18. N19
4	HIRS/3	Radiance	N16, N17
5	HIRS/4	Radiance	Metop-A, N18, N19
6	AIRS	Radiance	Aqua
7	SBUV8	Ozone	N16, N17, N18
8	GPSRO	Bending angle	COSMIC, GRAS
9	SPTRMM	Precipitation rates	TRMM, SSM/I *
10	AMSRE	Radiance	Aqua

Table 5: Category wise observations that are finally assimilated in gsi, a typical example on 23rd, Dec 2010 00z cycle.

Observation Type	**No.Observations (n)**	**Jo ***	**Jo/n**
surface pressure	28359	5.8818183794240749E+03	.207
temperature	78722	6.2883268538148484E+04	.826
moisture	12643	4.0967373019130400E+03	.284
precipitation	1086	9.4069356296249111E+01	.087
ozone	5368	1.5252320248366746E+03	.284
gps	27598	4.7786771608289644E+04	1.732
radiance	898328	1.6156444601691328E+05	.180
All	1248884	4.2407169637385121E+05	.340

*Jo is the weighted fit of the analysis to the observations

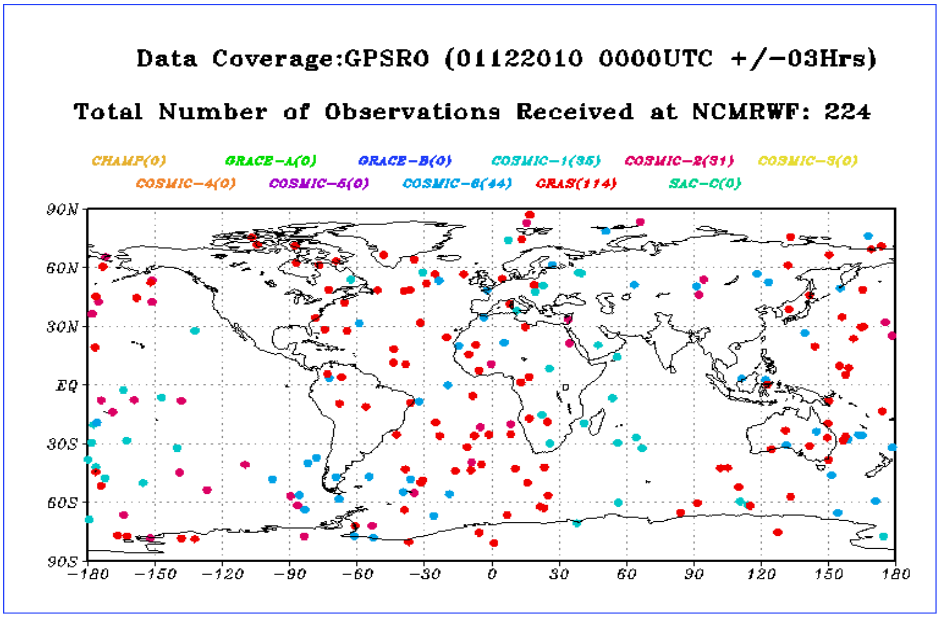

Fig. 2 GPSRO data coverage.

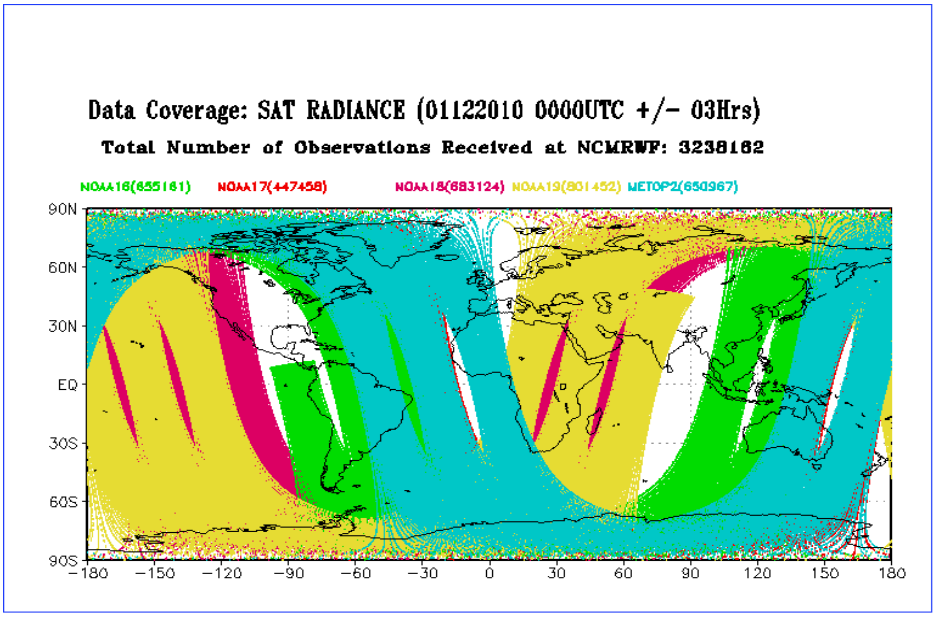

Fig. 3 Satellite radiance data coverage.

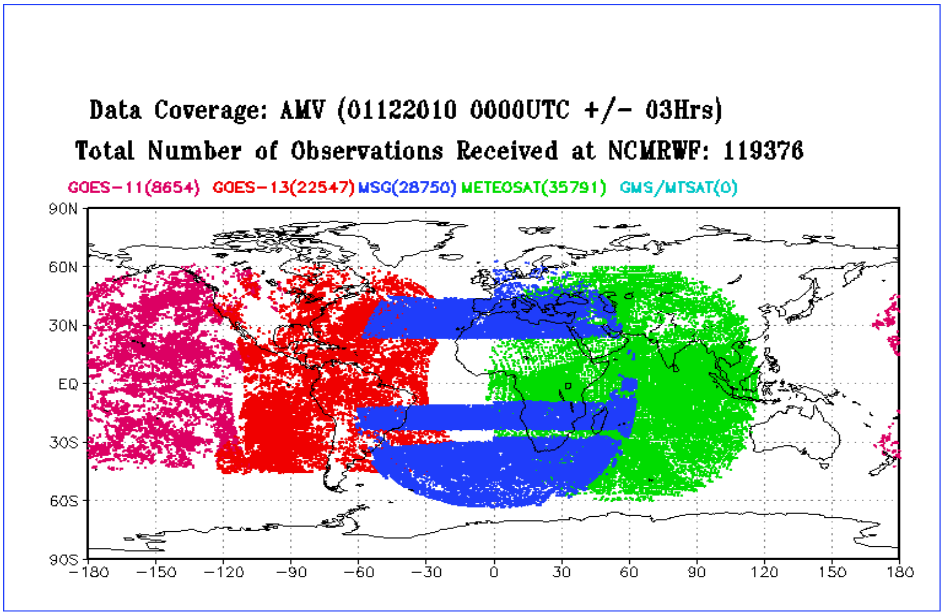

Fig. 4 AMV data coverage.

4. Forecast model

Rajagopal et al. (2007) gives a detailed description of the T254L64 GFS system which is operational from January, 2007 at NCMRWF. The new GFS forecast model is an upgraded version of NCEP GFS system (Kanamitsu, 1989; Kalnay et al., 1990; Kanamitsu, et al., 1991; Moorthi et al., 2001; EMC, 2003). History of changes to model, analysis and post processing of NCEP GFS are documented in the following link;

http://www.emc.ncep.noaa.gov/gmb/STATS/html/model_changes.html

An overview of the model is given in Table 6.

Table 6. Overview of the GFS model.

Dynamics: Spectral, Hybrid sigma-p, Reduced Gaussian grids
Time integration: Leapfrog/Semi-implicit
Time filter: Asselin (1972)
Horizontal diffusion: 8^{th} order wavenumber dependent
Orography: Mean orography (Hong,1999)
Surface fluxes: Monin-obhukov Similarity (Miyakoda and Sirutis,1986)
Turbulent fluxes: Non-local closure (Hong and Pan, 1996 ; Lock et al., 2000)
SW Radiation; RRTM (AER ; Iacono et al., 2000; Clough et al., 2005)
LW Radiation: RRTM (AER; Mlawer et al., 1997)
Deep Convection: SAS (Pan and Wu, 1995; Hong and Pan, 1998; Han and Pan, 2006)
Shallow convection: Mass-flux based (Han and Pan, 2010)
Grid-scale condensation: Zhao Microphysics (Zhao and Carr, 1997; Sundquist et al., 1989)
Land Surface Processes: 4-layer NOAH LSM (Ek et al., 2003)
Cloud fraction: Xu and Randal (1996)
Rainfall evaporation: Kessler (1969)
Air-sea interaction: Roughness length by Charnock(1955)
Gravity Wave Drag: Based on Alpert (Alpert et al., 1988; 1996; Kim and Arakawa, 1995)
Sea-Ice model: 3-layer thermodynamic model (Winton, 2000; Wu et al., 2005)

A brief summary of the major changes in the global forecast model is given below.

a. Resolution and model parameters:

New GFS system was implemented in May, 2010 at a resolution of Triangular truncation of 382 waves zonally and 64 levels in the vertical (T382L64). The Gaussian grid comprises of 1152x576 points with an average grid size of 35Km and the corresponding time step is 180 seconds. The model is run at a reduced grid with the 1152 equidistant grid points on the equator and 64 equidistant grid points near the pole (See Table 7 for the number of points at each Gaussian latitudes). It has a resolution of about 35Km over equator. It takes around 3 minutes for 24 hour forecast in 24x8 processors on IBM Power 6. A discussion of the upgradation of model resolution to T574L64 is provided in Section 7.

Table 7. The pole to equator number of grid points along the 288 Gaussian latitudes of the T382L64 reduced grid.

---

64 64 64 64 64 64 64 70 80 84
88 96 110 110 120 126 132 140 144 154
160 168 176 180 192 192 198 210 220 220
224 240 240 252 252 256 264 280 280 280
288 308 308 308 320 320 330 336 352 352
352 360 384 384 384 384 396 396 420 420
420 420 440 440 440 448 448 462 462 480
480 480 504 504 504 504 512 528 528 528
560 560 560 560 560 560 576 576 616 616
616 616 616 616 616 616 630 630 640 640
660 660 660 660 672 672 704 704 704 704
704 704 720 720 720 768 768 768 768 768
768 768 768 768 768 792 792 792 792 792
840 840 840 840 840 840 840 840 840 840
880 880 880 880 880 880 880 880 880 880

896 896 896 896 924 924 924 924 924 924
960 960 960 960 960 960 960 960 960 960
990 990 990 990 990 990 990 990 1008 1008
1008 1008 1008 1008 1024 1024 1024 1024 1024 1024
1056 1056 1056 1056 1056 1056 1056 1056 1056 1056
1120 1120 1120 1120 1120 1120 1120 1120 1120 1120
1120 1120 1120 1120 1120 1120 1120 1120 1120 1120
1120 1120 1120 1120 1120 1120 1120 1120 1120 1120
1120 1152 1152 1152 1152 1152 1152 1152 1152 1152
1152 1152 1152 1152 1152 1152 1152 1152 1152 1152
1152 1152 1152 1152 1152 1152 1152 1152 1152 1152
1152 1152 1152 1152 1152 1152 1152 1152 1152 1152
1152 1152 1152 1152 1152 1152 1152 1152 1152 1152
1152 1152 1152 1152 1152 1152 1152 1152

---

b. Vertical coordinate system:

Vertical coordinate was changed from sigma to hybrid sigma-pressure, reducing some upper air model errors (Sela, 2009). The hybrid coordinate system is terrain following in the lower levels and transforming to pure pressure levels in the upper levels and is uniquely represented by two values Ak and Bk at the interfaces. The values of (Ak*1000.0) and Bk are read from the fixed file global_hyblev.l64.txt. The interface pressure levels (in hPa) can be derived by the relation;

$$IPres(k) = (Ak + Bk * P0)*10.0$$

where P0 is the surface pressure in centibars (cb).

The layer pressures (Pres), sigma interface (SI) and sigma layer (SL) equivalents for dynamics can be derived from the relations:

$$Pres(k)=[1/(kappa+1)\ (IPres(k)**(kappa+1)-IPres(k+1)**(kappa+1))/(IPres(k)-IPres(k+1))]**(1/kappa)$$

$$SI(k) = (Ak/P0 +Bk)$$

$SL(k)=(SI(k) + SI(k+1))*0.5$ and $kappa=R_d/C_p$.

The Table 8 shows the above parameters for 64 level hybrid model for a standard P0=101.3cb.

Table 8: Hybrid sigma-p vertical levels for P0=101.3cb.

Level	AK	BK	IPres(hPa)	SI	SL	Pres(hPa)
64	.064247	.000000	.642470	.000634	.000317	.266594
63	.137790	.000000	1.377900	.001360	.000997	.993826
62	.221958	.000000	2.219580	.002191	.001776	1.786893
61	.318266	.000000	3.182660	.003142	.002666	2.690840
60	.428434	.000000	4.284340	.004229	.003686	3.723783
59	.554424	.000000	5.544240	.005473	.004851	4.904647
58	.698457	.000000	6.984570	.006895	.006184	6.254526
57	.863058	.000000	8.630580	.008520	.007707	7.797226
56	1.051080	.000000	10.510799	.010376	.009448	9.559677
55	1.265752	.000000	12.657519	.012495	.011435	11.572293
54	1.510711	.000000	15.107111	.014913	.013704	13.869452
53	1.790051	.000000	17.900509	.017671	.016292	16.489719
52	2.108366	.000000	21.083660	.020813	.019242	19.476591
51	2.470788	.000000	24.707880	.024391	.022602	22.878685
50	2.883038	.000000	28.830379	.028460	.026426	26.750189
49	3.351460	.000000	33.514599	.033085	.030772	31.151546
48	3.883052	.000000	38.830521	.038332	.035708	36.149311
47	4.485493	.000000	44.854931	.044279	.041306	41.816917
46	5.167146	.000000	51.671463	.051008	.047644	48.234432
45	5.937050	.000000	59.370499	.058609	.054808	55.489258
44	6.804874	.000000	68.048737	.067175	.062892	63.674412
43	7.777150	.000037	77.808945	.076810	.071993	72.889954

42	8.832537	.000431	88.762039	.087623	.082217	83.242531
41	9.936614	.001636	101.023323	.099727	.093675	94.845551
40	11.054852	.004107	114.708626	.113237	.106482	107.814285
39	12.152937	.008294	129.931213	.128264	.120750	122.263420
38	13.197065	.014637	146.798065	.144914	.136589	138.303543
37	14.154316	.023556	165.405273	.163283	.154098	156.035553
36	14.993074	.035442	185.833115	.183448	.173365	175.548447
35	15.683489	.050647	208.140137	.205469	.194459	196.911514
34	16.197968	.069475	232.357422	.229376	.217422	220.169495
33	16.511736	.092167	258.482422	.255165	.242270	245.337112
32	16.611603	.118812	286.472778	.282796	.268981	272.391785
31	16.503145	.149269	316.240723	.312182	.297489	301.269409
30	16.197315	.183296	347.652252	.343191	.327687	331.858093
29	15.708893	.220570	380.526550	.375643	.359417	364.001434
28	15.056342	.260685	414.637787	.409317	.392480	397.495117
27	14.261435	.303164	449.719604	.443948	.426632	432.093262
26	13.348671	.347468	485.472290	.479242	.461595	467.514618
25	12.344490	.393018	521.572388	.514879	.497061	503.445953
24	11.276348	.439211	557.684021	.550527	.532703	539.556152
23	10.171712	.485443	593.471191	.585855	.568191	575.512146
22	9.057051	.531135	628.610107	.620543	.603199	610.980286
21	7.956908	.575747	662.800415	.654295	.637419	645.649292
20	6.893117	.618800	695.775208	.686846	.670570	679.241394
19	5.884206	.659887	727.307678	.717974	.702410	711.500305
18	4.945029	.698683	757.216125	.747499	.732736	742.226624
17	4.086614	.734945	785.365662	.775287	.761393	771.259399
16	3.316217	.768515	811.667542	.801251	.788269	798.489258
15	2.637553	.799310	836.076294	.825347	.813299	823.854187
14	2.051150	.827319	858.585510	.847567	.836457	847.315735
13	1.554789	.852591	879.222290	.867939	.857753	868.885254
12	1.143988	.875224	898.041382	.886517	.877228	888.624023

11	.812489	.895355	915.119568	.903376	.894946	906.564392
10	.552720	.913151	930.549255	.918607	.910991	922.825256
9	.356223	.928797	944.433899	.932314	.925461	937.493774
8	.214015	.942491	956.883606	.944604	.938459	950.646057
7	.116899	.954434	968.010803	.955588	.950096	962.449585
6	.055712	.964828	977.927490	.965378	.960483	972.958984
5	.021516	.973868	986.743103	.974080	.969729	982.343628
4	.005741	.981742	994.562378	.981799	.977939	990.649597
3	.000575	.988627	1001.484497	.988632	.985216	998.025208
2	.000000	.994671	1007.601929	.994671	.991652	1004.550659
1	.000000	1.000000	1013.000000	1.000000	.997336	1010.295715

---

c. Upgraded ESMF library:

The Earth System Modelling Framework (ESMF) Library is upgraded to the version 3.1.0rp2.

d. Restructured GFS code

The GFS code is restructured to have many options for updated dynamics and physics and for code unification with global ensemble forecast system, etc. Also incorporated are the options to include the 3D diagnostics and GOCART outputs (for aerosol and dust model). The namelist options LDIAG3D and LGOC3D are to be set to ‘false’ in the Job file for operational runs as otherwise that makes the model run too slow.

The important dynamics and physics options can be given through the namelists in the Job file. The following list shows more or less full range of options employed for T382L64 with meanings of the some of the relevant options.

FHMAX=240.0, Model integration period (hours)
FHOUT=1.0, Output interval (hours)
FHRES=24.0, Restart file output interval (hours)
FHZER=6.0, Hours to accumulate the precipitation
FHSEG=0.0, Not in use
FHROT=0.0, Start from an initial single sigma file
DELTIM=180.0, Time-step in seconds
NGPTC=30, Chunk of longitudes on which physics operates
FHDFI=3.0, Hours to run digital filter Initialisation
FHSWR=1.0, SW radiation calling interval is 1 hour
FHLWR=3.0, LW radiation calling interval is 3 hours
FHCYC=24.0, Surface cycling interval (hours)
RAS=F, RAS convection not called
LGOC3D=F, Control for GOCART output (=false)
LDIAG3D=F, Control for 3D diagnostics(=false)
ADIAB=F, Switch for adiabatic run
EXPLICIT=F, No explicit time integration
PRE_RAD=F, Debug option to turn off radiation
HYBRID=T, Hybrid vertical coordinates
GEN_COORD_HYBRID=F, Not a generalized hybrid vertical coordinate
RANDOM_XKT2=T, Option for convective clouds – used by RAS and old SAS.
LIOPE=T, Option to turn on an IO processor.
RUN_ENTHALPY=F, Enthalpy as predict variable in place of Virtual Temperature
OUT_VIRTTEMP=T, Option for Virtual Temperature output (Default option)
NTRAC=3, Dimension variable for ozone array
JCAP=382, Spectral truncation
LEVS=64, No of model layers
LONF=1152, Number of Gaussian grid longitudes
LONR=1152, Number of Gaussian grid longitudes
LATG=576, Number of Gaussian grid latitudes
LATR=576, Number of Gaussian grid latitudes
LEVR=0, Optional radiation computation levels (if not LEVS)
NTOZ=2, Interactive ozone profile (>0); Climatological ozone (=0)
NTCW=3, Array location for cloud condensate (>0); No condensate (=0)
NCLD=1, Only used when ntcw > 0
LSOIL=4, Number of soil layers
NMTVR=14, Unit to read mountain variance
ZHAO_MIC=T, Switch for Zhao microphysics
NSOUT=0, Controls output frequency in timestep
LSM=1, Switch for NOAA LSM
TFILTC=0.849999999999999978, Time filter coefficient
ISOL=0, Prescribed solar constant
ICO2=0, Prescribed CO2 constant
IALB=0, Use climatology albedo based on surface type
IEMS=0, Black body (surface) emission (fixed value of 1.0 used)
IAER=0, Turn off aeorosol effect (Volcanic/LW/SW)

IOVR_SW=1, Maximum random cloud overlap (SW)
IOVR_LW=1, Maximum random cloud overlap (LW)
ICTM=1, Use external data at forecast time, or extrapolation
NCW=50, 150, For Ferrier microphysics (not active)
CRTRH=0.849999999999999978, 0.849999999999999978, 0.849999999999999978,
OLD_MONIN=T, Old PBL scheme
FLGMIN=0.200000000000000011, 0.200000000000000011, For Ferrier microphysics
GFSIO_IN=F, Options for sigma file IO on Gaussian grid
GFSIO_OUT=F, Options for sigma file IO on Gaussian grid
REF_TEMP=300.0, Reference temperature
CNVGWD=F, No convective GWD
CCWF=1.0, (For RAS only)
SASHAL=F, Logical flag for Jongil's shallow convection
NEWSAS=F, Old SAS scheme used.
ZFLXTVD=F, Switch for Van Leer flux-limited Vertical tracer advection
CRICK_PROOF=F, Cloud-Radiation Instability of Computational Kind (Not used)
CCNORM=F, Logical flag for incloud condensate mixing ratio
CTEI_RM=10.0, Alternate option for marine boundary layer clouds (Not operational)
MOM4ICE=F, Option for coupling to MOM4 Ocean model
NORAD_PRECIP=F, Option for radiation to take into account precip (for Ferrier/Moorthi)
NUM_REDUCE=-4, Reduced grids
MSTRAT=F, Option to get better marine boundary layer clouds (for old_monin)
TRANS_TRAC=T, Option for tracer transport through convection (for RAS)
NSST_ACTIVE=F, Options for coupling to near sea surface temperature model
NSST_RESTART=F, Options for coupling to near sea surface temperature model
TR_ANALYSIS=F, Options for coupling to near sea surface temperature model
LSEA=0, Options for coupling to near sea surface temperature model
CAL_PRE=F, Switch for Huiya's precipitation type algorithm
FHOUT_HF=1.00 High frequency output interval (hours)
FHMAX_HF=0.0 High frequency output period (hours)

e. Radiation and clouds:

- Output definition of low clouds was changed to combine the previously separately defined boundary-layer cloud and low cloud. High, Medium and Low clouds domain boundaries are adjusted for better agreement with observations (Hu et al., 2008; 2010; Wood and Bretherton, 2006).
- Short wave (SW) routine changed from ncep0 to RRTM2.
- Long wave (LW) computation frequency set as 1 hour.
- Added stratospheric aerosol (SW and LW) and tropospheric aerosol (LW).

- Aerosol single scattering albedo set as 0.99.
- SW aerosol asymmetry factor is changed and used new aerosol climatology.
- SW cloud overlap is changed from random to maximum random overlap.
- Used time varying global mean CO2 instead of constant CO2
- Treatment of the dependence of direct-beam surface albedo on solar zenith angle over snow-free land surface (Yang et al., 2008).

f. Gravity Wave Drag:

- Used a modified Gravity Wave Drag (GWD) routine, to automatically scale mountain block and GWD stress with resolution.
- Used four times stronger mountain block and one half the strength of GWD.

g. Planetary Boundary Layer:

- Included stratocumulus-top driven turbulence mixing.
- Enhanced stratocumulus-top driven diffusion for cloud top entrainment instability.
- Used local diffusion for night time stable Planetary Boundary Layer (PBL).
- Background diffusion in inversion layers 2.5Km over ocean is reduced by 70% to decrease the erosion of stratocumulus along the coastal area.
- Use of bulk-Richardson number to calculate PBL height.

h. Shallow convection:

- New Mass-flux shallow convection scheme.
- Detrain cloud water from every updraft layer. Convection starting level is defined as the level of maximum moist static energy within PBL.
- Cloud top is limited to 700 hPa.
- Entrainment rate is given to be inversely proportional to height and detrainment ratio is

set to be a constant as entrainment rate at the cloud base.

- Mass flux at the cloud base is given to be a function of convection boundary layer velocity scale.

i. Deep convection:

- Modified Simplified-Arakawa-Scheme.
- Eliminate Random cloud type, and cloud water is detrained from every cloud layer of the height cloud.
- Finite entrainment and detrainment rates for heat, moisture and momentum are specified.
- Similar to shallow convection scheme, entrainment rate is given to be inversely proportional to height in sub-cloud layers and detrainment rate is set to be a constant as entrainment rate at the cloud base.
- Above cloud base, an organized entrainment is added, which is a function of environmental relative humidity.
- Intraseasonal momentum background diffusivity for winds only.
- Convective overshooting increased cloud water detrainment in upper cloud layers.

j. Tracer transport scheme:

- Removal of negative water vapor using a positive-definite tracer transport scheme (Yang et al., 2009) in the vertical to replace the central-differencing scheme to eliminate computationally-induced negative tracers.
- Changing GSI factqmin and factqmax parameters to reduce negative water vapor and superstauration points from analysis steps.
- Modifying cloud physics to limit the borrowing of water vapor that is used to fill negative cloud water to the maximum amount of available water vapor so as to prevent the model from producing negative water vapor.
- The minimum value of water vapor mass mixing ration in the radiation is changed from 1.0e-5 to 1.0e-20. Otherwise the model artificially injects water vapor in the upper

atmosphere where water vapor mixing ratio is often below 1.0e-5.

5. Post processing

The main outputs of GFS models are 'sf', 'bf' and sfluxgrbf' files, in which the former two files are the binary restart files (sigma and surface boundary parameters) and the sfluxgrbf file contains the fluxes and surface parameters in grib1 format. 'sf' file contains the sigma levels parameters which need to be post processed to derive variables at specified pressure levels, and Gaussian to regular/standard grids (optional) and written in grib format. The post processed outputs are placed in the tree branch 'gfs/nwdata/post' inside the directories named with the corresponding date stamps. Surface flux grib (sfluxgrbf) files currently contain many new parameters added to it and a list of the parameters (total 109 records) is given in Table 9 below.

Table 9: File structure of sfluxgrbf file.

Variable	Level	Valid for	Description
UFLX	Sfc	18-24hr av	Zonal momentum flux [N/m**2]
VFLX	Sfc	18-24hr av	Meridional momentum flux [N/m**2]
SHTFL	Sfc	18-24hr av	Sensible heat flux [W/m**2]
LHTFL	Sfc	18-24hr av	Latent heat flux [W/m**2]
TMP	Sfc	24hr fcst	Temp. [K]
SOILW	0-10 cm down	24hr fcst	Volumetric soil moisture [fraction]
SOILW	10-40 cm down	24hr fcst	Volumetric soil moisture [fraction]
TMP	0-10 cm down	24hr fcst	Temp. [K]
TMP	10-40 cm down	24hr fcst	Temp. [K]
WEASD	Sfc	24hr fcst	Accum. snow [kg/m**2]
DLWRF	Sfc	18-24hr av	Downward long wave flux [W/m**2]
ULWRF	Sfc	18-24hr av	Upward long wave flux [W/m**2]
ULWRF	nom. Top	18-24hr av	Upward long wave flux [W/m**2]
USWRF	nom. Top	18-24hr av	Upward short wave flux [W/m**2]
USWRF	sfc	18-24hr av	Upward short wave flux [W/m**2]
DSWRF	sfc	18-24hr av	Downward short wave flux [W/m**2]
EVCW	sfc	18-24hr av	Canopy water evaporation [W/m**2]
ICWAT	Sfc	18-24hr av	Ice-free water surface [%]
TCDC	high cld lay	18-24hr av	Total cloud cover [%]
PRES	high cld top	18-24hr av	Pressure [Pa]
PRES	high cld bot	18-24hr av	Pressure [Pa]
TMP	high cld top	18-24hr av	Temp. [K]
TCDC	mid cld lay	18-24hr av	Total cloud cover [%]
PRES	mid cld top	18-24hr av	Pressure [Pa]

PRES	mid cld bot	18-24hr av	Pressure [Pa]
TMP	mid cld top	18-24hr av	Temp. [K]
TCDC	low cld lay	18-24hr av	Total cloud cover [%]
PRES	low cld top	18-24hr av	Pressure [Pa]
PRES	low cld bot	18-24hr av	Pressure [Pa]
TMP	low cld top	18-24hr av	Temp. [K]
PRATE	Sfc	18-24hr av	Precipitation rate [kg/m**2/s]
CPRAT	Sfc	18-24hr av	Convective precip. rate [kg/m**2/s]
GFLUX	Sfc	18-24hr av	Ground heat flux [W/m**2]
LAND	Sfc	24hr fcst	Land cover (land=1;sea=0) [fraction]
ICEC	Sfc	24hr fcst	Ice concentration (ice=1;no ice=0) [fraction]
UGRD	10 m ab. gnd	24hr fcst	u wind [m/s]
VGRD	10 m ab. gnd	24hr fcst	v wind [m/s]
TMP	2 m ab. Gnd	24hr fcst	Temp. [K]
SPFH	2 m ab. Gnd	24hr fcst	Specific humidity [kg/kg]
PRES	Sfc	24hr fcst	Pressure [Pa]
TMAX	2 m ab. Gnd	val 18-24hr	Max. temp. [K]
TMIN	2 m ab. Gnd	val 18-24hr	Min. temp. [K]
DSWRF	2 m ab. Gnd	val 18-24hr	Downward short wave flux [W/m**2]
DLWRF	2 m ab. Gnd	val 18-24hr	Downward long wave flux [W/m**2]
WATR	Sfc	18-24hr ac	Water runoff [kg/m**2]
PEVPR	Sfc	18-24hr av	Potential evaporation rate [W/m**2]
CWORK	atmos col	18-24hr av	Cloud work function [J/kg]
U-GWD	Sfc	18-24hr av	Zonal gravity wave stress [N/m**2]
V-GWD	Sfc	18-24hr av	Meridional gravity wave stress [N/m**2]
HPBL	Sfc	24hr fcst	Planetary boundary layer height [m]
PWAT	atmos col	24hr fcst	Precipitable water [kg/m**2]
ALBDO	Sfc	18-24hr av	Albedo [%]
TCDC	atmos col	18-24hr av	Total cloud cover [%]
TCDC	convect-cld layer	24hr fcst	Total cloud cover [%]
PRES	convect-cld top	24hr fcst	Pressure [Pa]
PRES	convect-cld bot	24hr fcst	Pressure [Pa]
TCDC	bndary-layer cld layer	18-24hr av	Total cloud cover [%]
ICETK	Sfc	24hr fcst	Ice thickness [m]
SOILW	40-100 cm down	24hr fcst	Volumetric soil moisture [fraction]
SOILW	100-200 cm down	24hr fcst	Volumetric soil moisture [fraction]
TMP	40-100 cm down	24hr fcst	Temp. [K]
TMP	100-200 cm down	24hr fcst	Temp. [K]
CSUSF	0-10 cm down	24hr fcst	Clear sky upward solar flux [W/m**2]
CSUSF	10-40 cm down	24hr fcst	Clear sky upward solar flux [W/m**2]
CSUSF	40-100 cm down	24hr fcst	Clear sky upward solar flux [W/m**2]
CSUSF	100-200 cm down	24hr fcst	Clear sky upward solar flux [W/m**2]
SNOD	Sfc	24hr fcst	Snow depth [m]
CNWAT	Sfc	24hr fcst	Plant canopy surface water [kg/m**2]
SFCR	Sfc	24hr fcst	Surface roughness [m]
VEG	Sfc	24hr fcst	Vegetation [%]
VGTYP	Sfc	24hr fcst	Vegetation type (as in SiB) [0..13]

SOTYP	Sfc	24hr fcst	Soil type (Zobler) [0..9]
5WAVH	Sfc	24hr fcst	5-wave geopotential height [gpm]
FRICV	Sfc	24hr fcst	Friction velocity [m/s]
HGT	Sfc	24hr fcst	Geopotential height [gpm]
CRAIN	Sfc	24hr fcst	Categorical rain [yes=1;no=0]
SFEXC	Sfc	24hr fcst	Exchange coefficient [(kg/m**3)(m/s)]
GRMR	Sfc	24hr fcst	Graupel mixing ratio
PEVPR	Sfc	24hr fcst	Potential evaporation rate [W/m**2]
DLWRF	Sfc	24hr fcst	Downward long wave flux [W/m**2]
ULWRF	Sfc	24hr fcst	Upward long wave flux [W/m**2]
USWRF	Sfc	24hr fcst	Upward short wave flux [W/m**2]
DSWRF	Sfc	24hr fcst	Downward short wave flux [W/m**2]
SHTFL	Sfc	24hr fcst	Sensible heat flux [W/m**2]
LHTFL	Sfc	24hr fcst	Latent heat flux [W/m**2]
GFLUX	Sfc	24hr fcst	Ground heat flux [W/m**2]
SSRUN	Sfc	18-24hr ac	Storm surface runoff [kg/m**2]
TMP	hybrid lev 1	24hr fcst	Temp. [K]
SPFH	hybrid lev 1	24hr fcst	Specific humidity [kg/kg]
UGRD	hybrid lev 1	24hr fcst	u wind [m/s]
VGRD	hybrid lev 1	24hr fcst	v wind [m/s]
HGT	hybrid lev 1	24hr fcst	Geopotential height [gpm]
EVBS	Sfc	18-24hr av	Direct evaporation from bare soil [W/m**2]
EVCW	Sfc	18-24hr av	Canopy water evaporation [W/m**2]
TRANS	Sfc	18-24hr av	Transpiration [W/m**2]
NCIP	Sfc	18-24hr av	No. concen. ice particles
SNOWC	Sfc	18-24hr av	Snow cover [%]
SOILM	0-200 cm down	24hr fcst	Soil moisture content [kg/m**2]
DSWRF	nom. Top	18-24hr av	Downward short wave flux [W/m**2]
CSULF	nom. Top	18-24hr av	Clear sky upward long wave flux [W/m**2]
CSUSF	nom. Top	18-24hr av	Clear sky upward solar flux [W/m**2]
CSDLF	Sfc	18-24hr av	Clear sky downward long wave flux [W/m**2]
CSUSF	Sfc	18-24hr av	Clear sky upward solar flux [W/m**2]
CSDSF	Sfc	18-24hr av	Clear sky downward solar flux [W/m**2]
CSULF	Sfc	18-24hr av	Clear sky upward long wave flux [W/m**2]
SNOHF	Sfc	18-24hr av	Snow phase-change heat flux [W/m**2]
TSD1D	Sfc	24hr fcst	Std. dev. of IR T over 1x1 deg area [K]
NLGSP	Sfc	24hr fcst	Natural log of surface pressure [ln(kPa)]
PROB	Sfc	18-24hr ac	Prob. from ensemble [non-dim]

The sigma file processing yields another pressure grib output file 'grbf'. There are two options for the post processing, POSTGP and NCEPPOST, the details of which are given in the following subsections.

a. POSTGP: This is the old post processor and currently not supported by NCEP. The

output latitude-longitudes need to be specified and it converts into regular latitude-longitude grids. Currently the T382L64 outputs are post processed at a resolution of 0.32 degree (1120x561) and the total record size is 432 (See the list in Table 10).

Table 10: File structure of grbf file.

Variable	Level	Valid for	Description
HGT	1000 mb	24hr fcst	Geopotential height [gpm]
HGT	975 mb	24hr fcst	Geopotential height [gpm]
HGT	950 mb	24hr fcst	Geopotential height [gpm]
HGT	925 mb	24hr fcst	Geopotential height [gpm]
HGT	900 mb	24hr fcst	Geopotential height [gpm]
HGT	850 mb	24hr fcst	Geopotential height [gpm]
HGT	800 mb	24hr fcst	Geopotential height [gpm]
HGT	750 mb	24hr fcst	Geopotential height [gpm]
HGT	700 mb	24hr fcst	Geopotential height [gpm]
HGT	650 mb	24hr fcst	Geopotential height [gpm]
HGT	600 mb	24hr fcst	Geopotential height [gpm]
HGT	550 mb	24hr fcst	Geopotential height [gpm]
HGT	500 mb	24hr fcst	Geopotential height [gpm]
HGT	450 mb	24hr fcst	Geopotential height [gpm]
HGT	400 mb	24hr fcst	Geopotential height [gpm]
HGT	350 mb	24hr fcst	Geopotential height [gpm]
HGT	300 mb	24hr fcst	Geopotential height [gpm]
HGT	250 mb	24hr fcst	Geopotential height [gpm]
HGT	200 mb	24hr fcst	Geopotential height [gpm]
HGT	150 mb	24hr fcst	Geopotential height [gpm]
HGT	100 mb	24hr fcst	Geopotential height [gpm]
HGT	70 mb	24hr fcst	Geopotential height [gpm]
HGT	50 mb	24hr fcst	Geopotential height [gpm]
HGT	30 mb	24hr fcst	Geopotential height [gpm]
HGT	20 mb	24hr fcst	Geopotential height [gpm]
HGT	10 mb	24hr fcst	Geopotential height [gpm]
TMP	1000 mb	24hr fcst	Temp. [K]
TMP	975 mb	24hr fcst	Temp. [K]
TMP	950 mb	24hr fcst	Temp. [K]
TMP	925 mb	24hr fcst	Temp. [K]
TMP	900 mb	24hr fcst	Temp. [K]
TMP	850 mb	24hr fcst	Temp. [K]
TMP	800 mb	24hr fcst	Temp. [K]
TMP	750 mb	24hr fcst	Temp. [K]
TMP	700 mb	24hr fcst	Temp. [K]
TMP	650 mb	24hr fcst	Temp. [K]
TMP	600 mb	24hr fcst	Temp. [K]
TMP	550 mb	24hr fcst	Temp. [K]
TMP	500 mb	24hr fcst	Temp. [K]

TMP	450 mb	24hr fcst	Temp. [K]
TMP	400 mb	24hr fcst	Temp. [K]
TMP	350 mb	24hr fcst	Temp. [K]
TMP	300 mb	24hr fcst	Temp. [K]
TMP	250 mb	24hr fcst	Temp. [K]
TMP	200 mb	24hr fcst	Temp. [K]
TMP	150 mb	24hr fcst	Temp. [K]
TMP	100 mb	24hr fcst	Temp. [K]
TMP	70 mb	24hr fcst	Temp. [K]
TMP	50 mb	24hr fcst	Temp. [K]
TMP	30 mb	24hr fcst	Temp. [K]
TMP	20 mb	24hr fcst	Temp. [K]
TMP	10 mb	24hr fcst	Temp. [K]
VVEL	1000 mb	24hr fcst	Pressure vertical velocity
VVEL	975 mb	24hr fcst	Pressure vertical velocit
VVEL	950 mb	24hr fcst	Pressure vertical velocit
VVEL	925 mb	24hr fcst	Pressure vertical velocit
VVEL	900 mb	24hr fcst	Pressure vertical velocit
VVEL	850 mb	24hr fcst	Pressure vertical velocit
VVEL	800 mb	24hr fcst	Pressure vertical velocit
VVEL	750 mb	24hr fcst	Pressure vertical velocit
VVEL	700 mb	24hr fcst	Pressure vertical velocit
VVEL	650 mb	24hr fcst	Pressure vertical velocit
VVEL	600 mb	24hr fcst	Pressure vertical velocit
VVEL	550 mb	24hr fcst	Pressure vertical velocit
VVEL	500 mb	24hr fcst	Pressure vertical velocit
VVEL	450 mb	24hr fcst	Pressure vertical velocit
VVEL	400 mb	24hr fcst	Pressure vertical velocit
VVEL	350 mb	24hr fcst	Pressure vertical velocit
VVEL	300 mb	24hr fcst	Pressure vertical velocit
VVEL	250 mb	24hr fcst	Pressure vertical velocit
VVEL	200 mb	24hr fcst	Pressure vertical velocit
VVEL	150 mb	24hr fcst	Pressure vertical velocit
VVEL	100 mb	24hr fcst	Pressure vertical velocit
RH	1000 mb	24hr fcst	Relative humidity [%]
RH	975 mb	24hr fcst	Relative humidity [%]
RH	950 mb	24hr fcst	Relative humidity [%]
RH	925 mb	24hr fcst	Relative humidity [%]
RH	900 mb	24hr fcst	Relative humidity [%]
RH	850 mb	24hr fcst	Relative humidity [%]
RH	800 mb	24hr fcst	Relative humidity [%]
RH	750 mb	24hr fcst	Relative humidity [%]
RH	700 mb	24hr fcst	Relative humidity [%]
RH	650 mb	24hr fcst	Relative humidity [%]
RH	600 mb	24hr fcst	Relative humidity [%]
RH	550 mb	24hr fcst	Relative humidity [%]
RH	500 mb	24hr fcst	Relative humidity [%]
RH	450 mb	24hr fcst	Relative humidity [%]

RH	400 mb	24hr fcst	Relative humidity [%]
RH	350 mb	24hr fcst	Relative humidity [%]
RH	300 mb	24hr fcst	Relative humidity [%]
RH	250 mb	24hr fcst	Relative humidity [%]
RH	200 mb	24hr fcst	Relative humidity [%]
RH	150 mb	24hr fcst	Relative humidity [%]
RH	100 mb	24hr fcst	Relative humidity [%]
ABSV	1000 mb	24hr fcst	Absolute vorticity [/s]
ABSV	975 mb	24hr fcst	Absolute vorticity [/s]
ABSV	950 mb	24hr fcst	Absolute vorticity [/s]
ABSV	925 mb	24hr fcst	Absolute vorticity [/s]
ABSV	900 mb	24hr fcst	Absolute vorticity [/s]
ABSV	850 mb	24hr fcst	Absolute vorticity [/s]
ABSV	800 mb	24hr fcst	Absolute vorticity [/s]
ABSV	750 mb	24hr fcst	Absolute vorticity [/s]
ABSV	700 mb	24hr fcst	Absolute vorticity [/s]
ABSV	650 mb	24hr fcst	Absolute vorticity [/s]
ABSV	600 mb	24hr fcst	Absolute vorticity [/s]
ABSV	550 mb	24hr fcst	Absolute vorticity [/s]
ABSV	500 mb	24hr fcst	Absolute vorticity [/s]
ABSV	450 mb	24hr fcst	Absolute vorticity [/s]
ABSV	400 mb	24hr fcst	Absolute vorticity [/s]
ABSV	350 mb	24hr fcst	Absolute vorticity [/s]
ABSV	300 mb	24hr fcst	Absolute vorticity [/s]
ABSV	250 mb	24hr fcst	Absolute vorticity [/s]
ABSV	200 mb	24hr fcst	Absolute vorticity [/s]
ABSV	150 mb	24hr fcst	Absolute vorticity [/s]
ABSV	100 mb	24hr fcst	Absolute vorticity [/s]
ABSV	70 mb	24hr fcst	Absolute vorticity [/s]
ABSV	50 mb	24hr fcst	Absolute vorticity [/s]
ABSV	30 mb	24hr fcst	Absolute vorticity [/s]
ABSV	20 mb	24hr fcst	Absolute vorticity [/s]
ABSV	10 mb	24hr fcst	Absolute vorticity [/s]
SPFH	1000 mb	24hr fcst	Specific humidity [kg/kg]
SPFH	975 mb	24hr fcst	Specific humidity [kg/kg
SPFH	950 mb	24hr fcst	Specific humidity [kg/kg
SPFH	925 mb	24hr fcst	Specific humidity [kg/kg
SPFH	900 mb	24hr fcst	Specific humidity [kg/kg
SPFH	850 mb	24hr fcst	Specific humidity [kg/kg
SPFH	800 mb	24hr fcst	Specific humidity [kg/kg
SPFH	750 mb	24hr fcst	Specific humidity [kg/kg
SPFH	700 mb	24hr fcst	Specific humidity [kg/kg
SPFH	650 mb	24hr fcst	Specific humidity [kg/kg
SPFH	600 mb	24hr fcst	Specific humidity [kg/kg
SPFH	550 mb	24hr fcst	Specific humidity [kg/kg
SPFH	500 mb	24hr fcst	Specific humidity [kg/kg
SPFH	450 mb	24hr fcst	Specific humidity [kg/kg
SPFH	400 mb	24hr fcst	Specific humidity [kg/kg

SPFH	350 mb	24hr fcst	Specific humidity [kg/kg
SPFH	300 mb	24hr fcst	Specific humidity [kg/kg
SPFH	250 mb	24hr fcst	Specific humidity [kg/kg
SPFH	200 mb	24hr fcst	Specific humidity [kg/kg
SPFH	150 mb	24hr fcst	Specific humidity [kg/kg
SPFH	100 mb	24hr fcst	Specific humidity [kg/kg
O3MR	100 mb	24hr fcst	Ozone mixing ratio [kg/kg]
O3MR	70 mb	24hr fcst	Ozone mixing ratio [kg/kg
O3MR	50 mb	24hr fcst	Ozone mixing ratio [kg/kg
O3MR	30 mb	24hr fcst	Ozone mixing ratio [kg/kg
O3MR	20 mb	24hr fcst	Ozone mixing ratio [kg/kg
O3MR	10 mb	24hr fcst	Ozone mixing ratio [kg/kg
CLWMR	1000 mb	24hr fcst	Cloud water [kg/kg]
CLWMR	975 mb	24hr fcst	Cloud water [kg/kg]
CLWMR	950 mb	24hr fcst	Cloud water [kg/kg]
CLWMR	925 mb	24hr fcst	Cloud water [kg/kg]
CLWMR	900 mb	24hr fcst	Cloud water [kg/kg]
CLWMR	850 mb	24hr fcst	Cloud water [kg/kg]
CLWMR	800 mb	24hr fcst	Cloud water [kg/kg]
CLWMR	750 mb	24hr fcst	Cloud water [kg/kg]
CLWMR	700 mb	24hr fcst	Cloud water [kg/kg]
CLWMR	650 mb	24hr fcst	Cloud water [kg/kg]
CLWMR	600 mb	24hr fcst	Cloud water [kg/kg]
CLWMR	550 mb	24hr fcst	Cloud water [kg/kg]
CLWMR	500 mb	24hr fcst	Cloud water [kg/kg]
CLWMR	450 mb	24hr fcst	Cloud water [kg/kg]
CLWMR	400 mb	24hr fcst	Cloud water [kg/kg]
CLWMR	350 mb	24hr fcst	Cloud water [kg/kg]
CLWMR	300 mb	24hr fcst	Cloud water [kg/kg]
CLWMR	250 mb	24hr fcst	Cloud water [kg/kg]
CLWMR	200 mb	24hr fcst	Cloud water [kg/kg]
CLWMR	150 mb	24hr fcst	Cloud water [kg/kg]
CLWMR	100 mb	24hr fcst	Cloud water [kg/kg]
5WAVH	500 mb	24hr fcst	5-wave geopotential height [gpm]
UGRD	1000 mb	24hr fcst	u wind [m/s]
UGRD	975 mb	24hr fcst	u wind [m/s]
UGRD	950 mb	24hr fcst	u wind [m/s]
UGRD	925 mb	24hr fcst	u wind [m/s]
UGRD	900 mb	24hr fcst	u wind [m/s]
UGRD	850 mb	24hr fcst	u wind [m/s]
UGRD	800 mb	24hr fcst	u wind [m/s]
UGRD	750 mb	24hr fcst	u wind [m/s]
UGRD	700 mb	24hr fcst	u wind [m/s]
UGRD	650 mb	24hr fcst	u wind [m/s]
UGRD	600 mb	24hr fcst	u wind [m/s]
UGRD	550 mb	24hr fcst	u wind [m/s]
UGRD	500 mb	24hr fcst	u wind [m/s]
UGRD	450 mb	24hr fcst	u wind [m/s]

UGRD	400 mb	24hr fcst	u wind [m/s]
UGRD	350 mb	24hr fcst	u wind [m/s]
UGRD	300 mb	24hr fcst	u wind [m/s]
UGRD	250 mb	24hr fcst	u wind [m/s]
UGRD	200 mb	24hr fcst	u wind [m/s]
UGRD	150 mb	24hr fcst	u wind [m/s]
UGRD	100 mb	24hr fcst	u wind [m/s]
UGRD	70 mb	24hr fcst	u wind [m/s]
UGRD	50 mb	24hr fcst	u wind [m/s]
UGRD	30 mb	24hr fcst	u wind [m/s]
UGRD	20 mb	24hr fcst	u wind [m/s]
UGRD	10 mb	24hr fcst	u wind [m/s]
VGRD	1000 mb	24hr fcst	v wind [m/s]
VGRD	975 mb	24hr fcst	v wind [m/s]
VGRD	950 mb	24hr fcst	v wind [m/s]
VGRD	925 mb	24hr fcst	v wind [m/s]
VGRD	900 mb	24hr fcst	v wind [m/s]
VGRD	850 mb	24hr fcst	v wind [m/s]
VGRD	800 mb	24hr fcst	v wind [m/s]
VGRD	750 mb	24hr fcst	v wind [m/s]
VGRD	700 mb	24hr fcst	v wind [m/s]
VGRD	650 mb	24hr fcst	v wind [m/s]
VGRD	600 mb	24hr fcst	v wind [m/s]
VGRD	550 mb	24hr fcst	v wind [m/s]
VGRD	500 mb	24hr fcst	v wind [m/s]
VGRD	450 mb	24hr fcst	v wind [m/s]
VGRD	400 mb	24hr fcst	v wind [m/s]
VGRD	350 mb	24hr fcst	v wind [m/s]
VGRD	300 mb	24hr fcst	v wind [m/s]
VGRD	250 mb	24hr fcst	v wind [m/s]
VGRD	200 mb	24hr fcst	v wind [m/s]
VGRD	150 mb	24hr fcst	v wind [m/s]
VGRD	100 mb	24hr fcst	v wind [m/s]
VGRD	70 mb	24hr fcst	v wind [m/s]
VGRD	50 mb	24hr fcst	v wind [m/s]
VGRD	30 mb	24hr fcst	v wind [m/s]
VGRD	20 mb	24hr fcst	v wind [m/s]
VGRD	10 mb	24hr fcst	v wind [m/s]
TMP	30-0 mb ab. Gnd	24hr fcst	Temp. [K]
TMP	60-30 mb ab. Gnd	24hr fcst	Temp. [K]
TMP	90-60 mb ab. Gnd	24hr fcst	Temp. [K]
TMP	120-90 mb ab. Gnd	24hr fcst	Temp. [K]
TMP	150-120 mb ab. Gnd	24hr fcst	Temp. [K]
TMP	180-150 mb ab. Gnd	24hr fcst	Temp. [K]
RH	30-0 mb ab. Gnd	24hr fcst	Relative humidity [%]
RH	60-30 mb ab. Gnd	24hr fcst	Relative humidity [%]
RH	90-60 mb ab. Gnd	24hr fcst	Relative humidity [%]
RH	120-90 mb ab. Gnd	24hr fcst	Relative humidity [%]

RH	150-120 mb ab. Gnd	24hr fcst	Relative humidity [%]
RH	180-150 mb ab. Gnd	24hr fcst	Relative humidity [%]
SPFH	30-0 mb ab. Gnd	24hr fcst	Specific humidity [kg/kg]
SPFH	60-30 mb ab. Gnd	24hr fcst	Specific humidity [kg/kg]
SPFH	90-60 mb ab. Gnd	24hr fcst	Specific humidity [kg/kg]
SPFH	120-90 mb ab. Gnd	24hr fcst	Specific humidity [kg/kg]
SPFH	150-120 mb ab. Gnd	24hr fcst	Specific humidity [kg/kg]
SPFH	180-150 mb ab. Gnd	24hr fcst	Specific humidity [kg/kg]
UGRD	30-0 mb ab. Gnd	24hr fcst	u wind [m/s]
UGRD	60-30 mb ab. Gnd	24hr fcst	u wind [m/s]
UGRD	90-60 mb ab. Gnd	24hr fcst	u wind [m/s]
UGRD	120-90 mb ab. Gnd	24hr fcst	u wind [m/s]
UGRD	150-120 mb ab. Gnd	24hr fcst	u wind [m/s]
UGRD	180-150 mb ab. Gnd	24hr fcst	u wind [m/s]
VGRD	30-0 mb ab. Gnd	24hr fcst	v wind [m/s]
VGRD	60-30 mb ab. Gnd	24hr fcst	v wind [m/s]
VGRD	90-60 mb ab. Gnd	24hr fcst	v wind [m/s]
VGRD	120-90 mb ab. Gnd	24hr fcst	v wind [m/s]
VGRD	150-120 mb ab. Gnd	24hr fcst	v wind [m/s]
VGRD	180-150 mb ab. Gnd	24hr fcst	v wind [m/s]
TMP	305 m ab. MSL	24hr fcst	Temp. [K]
TMP	457 m ab. MSL	24hr fcst	Temp. [K]
TMP	610 m ab. MSL	24hr fcst	Temp. [K]
TMP	914 m ab. MSL	24hr fcst	Temp. [K]
TMP	1829 m ab. MSL	24hr fcst	Temp. [K]
TMP	2743 m ab. MSL	24hr fcst	Temp. [K]
TMP	3658 m ab. MSL	24hr fcst	Temp. [K]
TMP	4572 m ab. MSL	24hr fcst	Temp. [K]
UGRD	305 m ab. MSL	24hr fcst	u wind [m/s]
UGRD	457 m ab. MSL	24hr fcst	u wind [m/s]
UGRD	610 m ab. MSL	24hr fcst	u wind [m/s]
UGRD	914 m ab. MSL	24hr fcst	u wind [m/s]
UGRD	1829 m ab. MSL	24hr fcst	u wind [m/s]
UGRD	2743 m ab. MSL	24hr fcst	u wind [m/s]
UGRD	3658 m ab. MSL	24hr fcst	u wind [m/s]
UGRD	4572 m ab. MSL	24hr fcst	u wind [m/s]
VGRD	305 m ab. MSL	24hr fcst	v wind [m/s]
VGRD	457 m ab. MSL	24hr fcst	v wind [m/s]
VGRD	610 m ab. MSL	24hr fcst	v wind [m/s]
VGRD	914 m ab. MSL	24hr fcst	v wind [m/s]
VGRD	1829 m ab. MSL	24hr fcst	v wind [m/s]
VGRD	2743 m ab. MSL	24hr fcst	v wind [m/s]
VGRD	3658 m ab. MSL	24hr fcst	v wind [m/s]
VGRD	4572 m ab. MSL	24hr fcst	v wind [m/s]
HGT	500 (pv units)	24hr fcst	Geopotential height [gpm]
HGT	33268 (pv units)	24hr fcst	Geopotential height [gpm]
HGT	1000 (pv units)	24hr fcst	Geopotential height [gpm]
HGT	33768 (pv units)	24hr fcst	Geopotential height [gpm]

HGT	1500 (pv units)	24hr fcst	Geopotential height [gpm]
HGT	34268 (pv units)	24hr fcst	Geopotential height [gpm]
HGT	2000 (pv units)	24hr fcst	Geopotential height [gpm]
HGT	34768 (pv units)	24hr fcst	Geopotential height [gpm]
TMP	500 (pv units)	24hr fcst	Temp. [K]
TMP	33268 (pv units)	24hr fcst	Temp. [K]
TMP	1000 (pv units)	24hr fcst	Temp. [K]
TMP	33768 (pv units)	24hr fcst	Temp. [K]
TMP	1500 (pv units)	24hr fcst	Temp. [K]
TMP	34268 (pv units)	24hr fcst	Temp. [K]
TMP	2000 (pv units)	24hr fcst	Temp. [K]
TMP	34768 (pv units)	24hr fcst	Temp. [K]
PRES	500 (pv units)	24hr fcst	Pressure [Pa]
PRES	33268 (pv units)	24hr fcst	Pressure [Pa]
PRES	1000 (pv units)	24hr fcst	Pressure [Pa]
PRES	33768 (pv units)	24hr fcst	Pressure [Pa]
PRES	1500 (pv units)	24hr fcst	Pressure [Pa]
PRES	34268 (pv units)	24hr fcst	Pressure [Pa]
PRES	2000 (pv units)	24hr fcst	Pressure [Pa]
PRES	34768 (pv units)	24hr fcst	Pressure [Pa]
VWSH	500 (pv units)	24hr fcst	Vertical speed shear [1/s]
VWSH	33268 (pv units)	24hr fcst	Vertical speed shear [1/s]
VWSH	1000 (pv units)	24hr fcst	Vertical speed shear [1/s]
VWSH	33768 (pv units)	24hr fcst	Vertical speed shear [1/s]
VWSH	1500 (pv units)	24hr fcst	Vertical speed shear [1/s]
VWSH	34268 (pv units)	24hr fcst	Vertical speed shear [1/s]
VWSH	2000 (pv units)	24hr fcst	Vertical speed shear [1/s]
VWSH	34768 (pv units)	24hr fcst	Vertical speed shear [1/s]
UGRD	500 (pv units)	24hr fcst	u wind [m/s]
UGRD	33268 (pv units)	24hr fcst	u wind [m/s]
UGRD	1000 (pv units)	24hr fcst	u wind [m/s]
UGRD	33768 (pv units)	24hr fcst	u wind [m/s]
UGRD	1500 (pv units)	24hr fcst	u wind [m/s]
UGRD	34268 (pv units)	24hr fcst	u wind [m/s]
UGRD	2000 (pv units)	24hr fcst	u wind [m/s]
UGRD	34768 (pv units)	24hr fcst	u wind [m/s]
VGRD	500 (pv units)	24hr fcst	v wind [m/s]
VGRD	33268 (pv units)	24hr fcst	v wind [m/s]
VGRD	1000 (pv units)	24hr fcst	v wind [m/s]
VGRD	33768 (pv units)	24hr fcst	v wind [m/s]
VGRD	1500 (pv units)	24hr fcst	v wind [m/s]
VGRD	34268 (pv units)	24hr fcst	v wind [m/s]
VGRD	2000 (pv units)	24hr fcst	v wind [m/s]
VGRD	34768 (pv units)	24hr fcst	v wind [m/s]
PRES	Sfc	24hr fcst	Pressure [Pa]
PWAT	atmos col	24hr fcst	Precipitable water [kg/m**2]
RH	atmos col	24hr fcst	Relative humidity [%]
HGT	Tropopause	24hr fcst	Geopotential height [gpm]

TMP	Tropopause	24hr fcst	Temp. [K]
PRES	Tropopause	24hr fcst	Pressure [Pa]
VWSH	Tropopause	24hr fcst	Vertical speed shear [1/s]
LFTX	Sfc	24hr fcst	Surface lifted index [K]
CAPE	Sfc	24hr fcst	Convective Avail. Pot. Energy [J/kg]
CIN	Sfc	24hr fcst	Convective inhibition [J/kg]
4LFTX	Sfc	24hr fcst	Best (4-layer) lifted index [K]
CAPE	180-0 mb ab. gnd	24hr fcst	Convective Avail. Pot. Energy [J/kg]
CIN	180-0 mb ab. gnd	24hr fcst	Convective inhibition [J/kg]
HGT	max wind lev	24hr fcst	Geopotential height [gpm]
TMP	max wind lev	24hr fcst	Temp. [K]
PRES	max wind lev	24hr fcst	Pressure [Pa]
HGT	Sfc	24hr fcst	Geopotential height [gpm]
PRMSL	MSL	24hr fcst	Pressure reduced to MSL [Pa]
RH	sigma 0.44-1.00	24hr fcst	Relative humidity [%]
RH	sigma 0.72-0.94	24hr fcst	Relative humidity [%]
RH	sigma 0.44-0.72	24hr fcst	Relative humidity [%]
RH	sigma 0.33-1.00	24hr fcst	Relative humidity [%]
POT	sigma=0.9950	24hr fcst	Potential temp. [K]
TMP	sigma=0.9950	24hr fcst	Temp. [K]
VVEL	sigma=0.9950	24hr fcst	Pressure vertical velocity [Pa/s]
RH	sigma=0.9950	24hr fcst	Relative humidity [%]
TOZNE	atmos col	24hr fcst	Total ozone [Dobson]
CWAT	atmos col	24hr fcst	Cloud water [kg/m**2]
HGT	0C isotherm	24hr fcst	Geopotential height [gpm]
RH	0C isotherm	24hr fcst	Relative humidity [%]
HGT		24hr fcst	Geopotential height [gpm]
RH		24hr fcst	Relative humidity [%]
UGRD	Tropopause	24hr fcst	u wind [m/s]
UGRD	max wind lev	24hr fcst	u wind [m/s]
UGRD	sigma=0.9950	24hr fcst	u wind [m/s]
VGRD	Tropopause	24hr fcst	v wind [m/s]
VGRD	max wind lev	24hr fcst	v wind [m/s]
VGRD	sigma=0.9950	24hr fcst	v wind [m/s]
SHTFL	Sfc	18-24hr av	Sensible heat flux [W/m**2]
LHTFL	Sfc	18-24hr av	Latent heat flux[W/m**2]
TMP	Sfc	24hr fcst	Temp. [K]
SOILW	0-10 cm down	24hr fcst	Volumetric soil moisture[fraction]
SOILW	10-40 cm down	24hr fcst	Volumetric soil moisture [fraction]
SOILW	40-100 cm down	24hr fcst	Volumetric soil moisture [fraction]
SOILW	100-200 cm down	24hr fcst	Volumetric soil moisture [fraction]
TMP	0-10 cm down	24hr fcst	Temp. [K]
TMP	10-40 cm down	24hr fcst	Temp. [K]

TMP	40-100 cm down	24hr fcst	Temp. [K]
TMP	100-200 cm down	24hr fcst	Temp. [K]
CSUSF	0-10 cm down	24hr fcst	Clear sky upward solar flux [W/m**2]
CSUSF	10-40 cm down	24hr fcst	Clear sky upward solar flux [W/m**2]
CSUSF	40-100 cm down	24hr fcst	Clear sky upward solar flux [W/m**2]
CSUSF	100-200 cm down	24hr fcst	Clear sky upward solar flux [W/m**2]
CNWAT	Sfc	24hr fcst	Plant canopy surface water [kg/m**2]
SNOD	Sfc	24hr fcst	Snow depth [m]
WEASD	Sfc	24hr fcst	Accum. snow [kg/m**2]
DLWRF	Sfc	18-24hr av	Downward long wave flux [W/m**2]
ULWRF	Sfc	18-24hr av	Upward long wave flux [W/m**2]
ULWRF	nom. Top	18-24hr av	Upward long wave flux [W/m**2]
USWRF	nom. Top	18-24hr av	Upward short wave flux [W/m**2]
USWRF	Sfc	18-24hr av	Upward short wave flux [W/m**2]
DSWRF	Sfc	18-24hr av	Downward short wave flux [W/m**2]
EVCW	Sfc	18-24hr av	Canopy water evaporation [W/m**2]
ICWAT	Sfc	18-24hr av	Ice-free water surface [%]
TCDC	high cld lay	18-24hr av	Total cloud cover [%]
PRES	high cld top	18-24hr av	Pressure [Pa]
PRES	high cld bot	18-24hr av	Pressure [Pa]
TMP	high cld top	18-24hr av	Temp. [K]
TCDC	mid cld lay	18-24hr av	Total cloud cover [%]
PRES	mid cld top	18-24hr av	Pressure [Pa]
PRES	mid cld bot	18-24hr av	Pressure [Pa]
TMP	mid cld top	18-24hr av	Temp. [K]
TCDC	low cld lay	18-24hr av	Total cloud cover [%]
PRES	low cld top	18-24hr av	Pressure [Pa]
PRES	low cld bot	18-24hr av	Pressure [Pa]
TMP	low cld top	18-24hr av	Temp. [K]
PRATE	Sfc	18-24hr av	Precipitation rate [kg/m**2/s]
CPRAT	Sfc	18-24hr av	Convective precip. rate [kg/m**2/s]
GFLUX	Sfc	18-24hr av	Ground heat flux [W/m**2]
LAND	Sfc	24hr fcst	Land cover (land=1;sea=0) [fraction]
ICEC	Sfc	24hr fcst	Ice concentration (ice=1;no ice=0) [fraction]
ICETK	Sfc	24hr fcst	Ice thickness [m]
TMP	2 m ab. Gnd	24hr fcst	Temp. [K]
SPFH	2 m ab. Gnd	24hr fcst	Specific humidity [kg/kg]
TMAX	2 m ab. Gnd	val 18-24hr	Max. temp. [K]

TMIN	2 m ab. Gnd	val 18-24hr	Min. temp. [K]
WATR	Sfc	18-24hr ac	Water runoff [kg/m**2]
PEVPR	Sfc	18-24hr av	Potential evaporation rate [W/m**2]
CWORK	atmos col	18-24hr av	Cloud work function [J/kg]
HPBL	Sfc	24hr fcst	Planetary boundary layer height [m]
ALBDO	Sfc	18-24hr av	Albedo [%]
TCDC	atmos col	18-24hr av	Total cloud cover [%]
TCDC	convect-cld layer	24hr fcst	Total cloud cover [%]
PRES	convect-cld top	24hr fcst	Pressure [Pa]
PRES	convect-cld bot	24hr fcst	Pressure [Pa]
TCDC	bndary-layer cld layer	18-24hr av	Total cloud cover [%]
APCP	Sfc	18-24hr ac	Total precipitation [kg/m**2]
ACPCP	Sfc	18-24hr ac	Convective precipitation [kg/m**2]
CRAIN	Sfc	18-24hr av	Categorical rain [yes=1;no=0]
CFRZR	Sfc	18-24hr av	Categorical freezing rain [yes=1;no=0]
CICEP	Sfc	18-24hr av	Categorical ice pellets [yes=1;no=0]
CSNOW	Sfc	18-24hr av	Categorical snow [yes=1;no=0]
RH	2 m ab. Gnd	24hr fcst	Relative humidity [%]
UFLX	Sfc	18-24hr av	Zonal momentum flux [N/m**2]
UGRD	10 m ab. Gnd	24hr fcst	u wind [m/s]
U-GWD	Sfc	18-24hr av	Zonal gravity wave stress [N/m**2]
VFLX	Sfc	18-24hr av	Meridional momentum flux [N/m**2]
VGRD	10 m ab. Gnd	24hr fcst	v wind [m/s]
V-GWD	Sfc	18-24hr av	Meridional gravity wave stress [N/m**2]

b. NCEPPOST: This is a unified post processor and outputs much more diagnostics than POSTGP. Some of formulations (like, freezing level calculation and precipitation type calculation) have been changed or fixed to be more accurate whereas POSTGP outputs are more smoothed out. Several new parameters have been added (like, RH at tropopause levels, ICAO height at the tropopause and maximum wind level and sunshine duration) and the output files are written in 1760x880 grid points (total 666 records). Initially CHGRES program is run to convert the sigma file output into the grib format and the record structure readable by NCEPPOST. The CHGRES step is very computationally expensive (unless the CHGRES is made to run faster by increasing the number of THREADS). All the multilevel fields are written every 25 hPa interval in place of 50 hPa interval as set in POSTGP. Apart from this difference, a number of new

parameters are computed by NCEPPOST in addition to the parameters listed in Table 10, which are listed in Table 11.

Table 11: List of additional parameters written in grbf file (thru NCEPPOST).

Variable	Level	Valid for	Description
VIS	Sfc	24hr fcst	Visibility [m]
O3MR	1 mb	24hr fcst	Ozone mixing ratio [kg/kg]
O3MR	2 mb	24hr fcst	Ozone mixing ratio [kg/kg]
O3MR	3 mb	24hr fcst	Ozone mixing ratio [kg/kg]
O3MR	5 mb	24hr fcst	Ozone mixing ratio [kg/kg]
O3MR	7 mb	24hr fcst	Ozone mixing ratio [kg/kg]
O3MR	10 mb	24hr fcst	Ozone mixing ratio [kg/kg]
O3MR	20 mb	24hr fcst	Ozone mixing ratio [kg/kg]
O3MR	30 mb	24hr fcst	Ozone mixing ratio [kg/kg]
O3MR	50 mb	24hr fcst	Ozone mixing ratio [kg/kg]
O3MR	70 mb	24hr fcst	Ozone mixing ratio [kg/kg]
O3MR	100 mb	24hr fcst	Ozone mixing ratio [kg/kg]
O3MR	125 mb	24hr fcst	Ozone mixing ratio [kg/kg]
DPT	2 m ab. gnd	24hr fcst	Dew point temp. [K]:
SFCR	Sfc	24hr fcst	Surface roughness [m]
FRICV	Sfc	24hr fcst	Friction velocity [m/s]
TSD1D	Sfc	24hr fcst	Std. dev. of IR T over 1x1 deg area [K]
NLGSP	Sfc	24hr fcst	Natural log of surface pressure [ln(kPa)]
PROB	Sfc	24hr fcst	Prob. from ensemble [non-dim]
HLCY	3000-0 m ab. gnd	24hr fcst	Storm relative helicity [m^2/s^2]:
HLCY	1000-0 m ab. gnd	24hr fcst	Storm relative helicity [m^2/s^2]:
USTM	6000-0 m ab. gnd	24hr fcst	u-component of storm motion [m/s]:
VSTM	6000-0 m ab. gnd	24hr fcst	v-component of storm motion [m/s]:
ICAHT	tropopause	24hr fcst	ICAO Standard Atmosphere Reference Height [M]
ICAHT	max wind lev	24hr fcst	ICAO Standard Atmosphere Reference Height [M]:
DPT	30-0 mb ab. gnd	24hr fcst	Dew point temp. [K]:
PLI	30-0 mb ab. gnd	24hr fcst	Parcel lifted index (to 500 hPa) [K]:
PVORT	320K	24hr fcst	Pot. vorticity [km^2/kg/s]
MNTSF	320K	24hr fcst	Montgomery stream function [m^2/s^2]
GPA	1000 mb	24hr fcst	Geopotential height anomaly [gpm]
GPA	500 mb	24hr fcst	Geopotential height anomaly [gpm]
5WAVA	500 mb	24hr fcst	5-wave geopot. height anomaly [gpm]
TCDC	475 mb	24hr fcst	Total cloud cover [%]
CLWMR	1 mb	24hr fcst	Geopotential height [gpm]
CLWMR	2 mb	24hr fcst	Geopotential height [gpm]
CLWMR	3 mb	24hr fcst	Geopotential height [gpm]
CLWMR	5 mb	24hr fcst	Geopotential height [gpm]
CLWMR	7 mb	24hr fcst	Geopotential height [gpm]
HGT	1 mb	24hr fcst	Geopotential height [gpm]

HGT	2 mb	24hr fcst	Geopotential height [gpm]
HGT	3 mb	24hr fcst	Geopotential height [gpm]
HGT	5 mb	24hr fcst	Geopotential height [gpm]
HGT	7 mb	24hr fcst	Geopotential height [gpm]
RH	1 mb	24hr fcst	Relative humidity [%]
RH	2 mb	24hr fcst	Relative humidity [%]
RH	3 mb	24hr fcst	Relative humidity [%]
RH	5 mb	24hr fcst	Relative humidity [%]
RH	7 mb	24hr fcst	Relative humidity [%]
RH	10 mb	24hr fcst	Relative humidity [%]
RH	20 mb	24hr fcst	Relative humidity [%]
RH	30 mb	24hr fcst	Relative humidity [%]
RH	50 mb	24hr fcst	Relative humidity [%]
RH	70 mb	24hr fcst	Relative humidity [%]
RH	125 mb	24hr fcst	Relative humidity [%]
TMP	1 mb	24hr fcst	Temp. [K]
TMP	2 mb	24hr fcst	Temp. [K]
TMP	3 mb	24hr fcst	Temp. [K]
TMP	5 mb	24hr fcst	Temp. [K]
TMP	7 mb	24hr fcst	Temp. [K]
BRTMP	nom. Top	24hr fcst	Brightness temperature [K]
TMP	320K	24hr fcst	Temp. [K]
UGRD	1 mb	24hr fcst	u wind [m/s]
UGRD	2 mb	24hr fcst	u wind [m/s]
UGRD	3 mb	24hr fcst	u wind [m/s]
UGRD	5 mb	24hr fcst	u wind [m/s]
UGRD	7 mb	24hr fcst	u wind [m/s]
UGRD	320K	24hr fcst	u wind [m/s]
VGRD	1 mb	24hr fcst	u wind [m/s]
VGRD	2 mb	24hr fcst	u wind [m/s]
VGRD	3 mb	24hr fcst	u wind [m/s]
VGRD	5 mb	24hr fcst	u wind [m/s]
VGRD	7 mb	24hr fcst	u wind [m/s]
VGRD	320K	24hr fcst	u wind [m/s]
SPFH	1 mb	24hr fcst	Specific humidity [kg/kg]
SPFH	2 mb	24hr fcst	Specific humidity [kg/kg]
SPFH	3 mb	24hr fcst	Specific humidity [kg/kg]
SPFH	5 mb	24hr fcst	Specific humidity [kg/kg]
SPFH	7 mb	24hr fcst	Specific humidity [kg/kg]
SPFH	10 mb	24hr fcst	Specific humidity [kg/kg]
SPFH	20 mb	24hr fcst	Specific humidity [kg/kg]
SPFH	30 mb	24hr fcst	Specific humidity [kg/kg]
SPFH	50 mb	24hr fcst	Specific humidity [kg/kg]
SPFH	70 mb	24hr fcst	Specific humidity [kg/kg]
ABSV	1 mb	24hr fcst	Absolute vorticity [/s]
ABSV	2 mb	24hr fcst	Absolute vorticity [/s]
ABSV	3 mb	24hr fcst	Absolute vorticity [/s]
ABSV	5 mb	24hr fcst	Absolute vorticity [/s]

ABSV	7 mb		24hr fcst	Absolute vorticity [/s]

After the post processing, the gribbed fields can be visualised using various softwares. The operational plots are set up with GrADS (Grid Analysis and Display System) software. The resources for the visualisation are kept in a separate subdirectory inside 'nwprod', with the name 'plot'. The directory 'gfs/nwprod/plot' contains two subdirectories, named 'scripts' (containing the main shell scripts) and 'util' (containing necessary GrADS scripts, utilities and accessories). The required shell scripts inside the 'gfs/nwprod/plot/scripts' area are being submitted within the post processing scripts (in 'gfs/nwprod/scripts' area) simultaneously with the post processing. The final plots are copied to area 'gfs/nwplot' in the respective location.

6. Case studies

The T382L64 system is run from May, 2010 on experimental mode for a forecast lead time of 10 days while T254L64 system being run for a forecast lead time of 7 days operationally. Two cases have been picked up for the comparative performance of T254L64 and T382L64 systems. One is a Monsoon-2010 case of low pressure area (LPA) during 30-31 August, 2010. The second is an event of Tropical Cyclone over southwest Bay of Bengal during 5-6, November, 2010. T382L64 was run with the options listed in Section 4d. The details of the cases are given below.

a. Low Pressure Area (30-31 August, 2010):

Monsoon-2010 has witnessed no single depression events, but a number of Low Pressure Areas (LPA) made the Monsoon normal with copious rainfall from LPAs occurring during July- September, 2010. Out of four LPAs formed in August, 2010, the two of them formed during the first fortnight period and after that the monsoon circulation remained week. the two LPAs that formed during the last week of August, 2010 made way for vigorous monsoon activity over many parts of the country. The last LPA of the month formed during 30-31 August, 2010 over northwest Bay of Bengal and subsequently moved west-northwest ward

giving rainfall over central India.

Fig. 5 depicts the wind and geopotential valid for 00Z 0f 30 August 2010. T382L64 forecast of days 3, 5 and 7 are plotted against the verifying analysis from the same system. The day-3 forecast shows slightly more intense system compared to the analysis whereas the Day-5 forecast gives better match with analysis. Though the location of Day-7 forecast is slightly displaced over to the land, in general the system was predicted satisfactorily. Fig. 6 is the corresponding plot for T254L64 system. In general T254L64 analysis and day-3 show more intense system compared to T382L64. However, comparing the intensity and location, T254L64 shows less perfect match with the corresponding analysis compared to T382L64 system. In fact Day-5 and Day-7 forecast show less intense fields compared to the corresponding analysis. Here also the Day-7 forecast is found to be more over land.

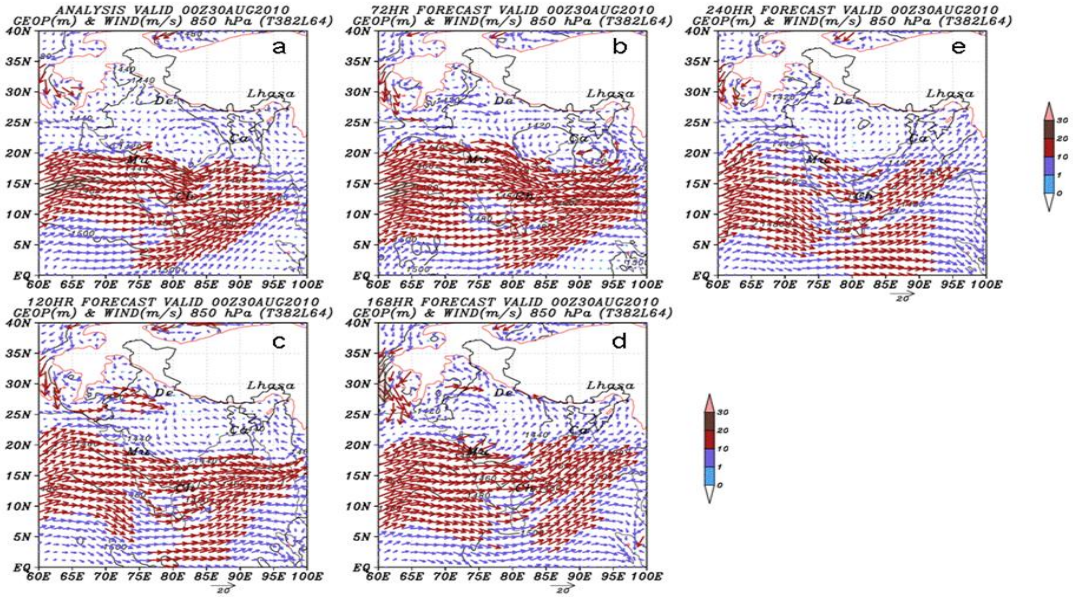

Fig. 5 Wind (m/s) and Geopotential (m) valid for 00Z 30 August, 2010; (a) analysis (b) Day-3 forecast (c) Day-5 forecast (d) Day-7 and (e) Day-10 forecast, all from T382L64 system.

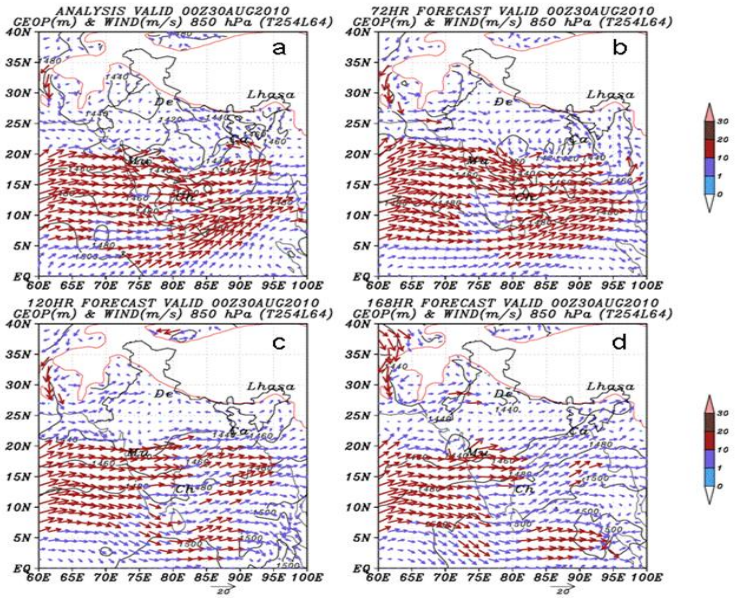

Fig. 6 Wind (m/s) and Geopotential (m) valid for 00Z 30 August, 2010; (a) analysis (b) Day-3 forecast (c) Day-5 forecast and (d) Day-7 forecast, all from T254L64 system.

Fig. 7 and 8 show the corresponding rainfall forecasts against TRMM 3B42RT derived daily rainfall data. The TRMM rainfall estimates are showing more activities concentrated over the western states of Maharashtra and Gujarat while the Day-3 forecast is concentrated over Chattisgurh and Orissa in T382L64 system due to the eastward location of rainfall activity in T382L64 predictions. In general, Day-5 and Day-7 show better match with the observations for T382L64 system compared to Day-3 in this particular case. However, for T254L64 case, all the forecast panels show poorer match with the observed rainfall, and only Day-3 shows any resemblance with the observed pattern. T254L64 model under predicted the intensity of the depression in Day-5 and Day-7 predictions which is reflected in the relatively lean rainfall patches compared to T382L64. Even the Day-10 forecast from T382L64 model does give some indication of the low pressure area. Thus in this case, T382L64 could predict the system 10 days in advance fairly well.

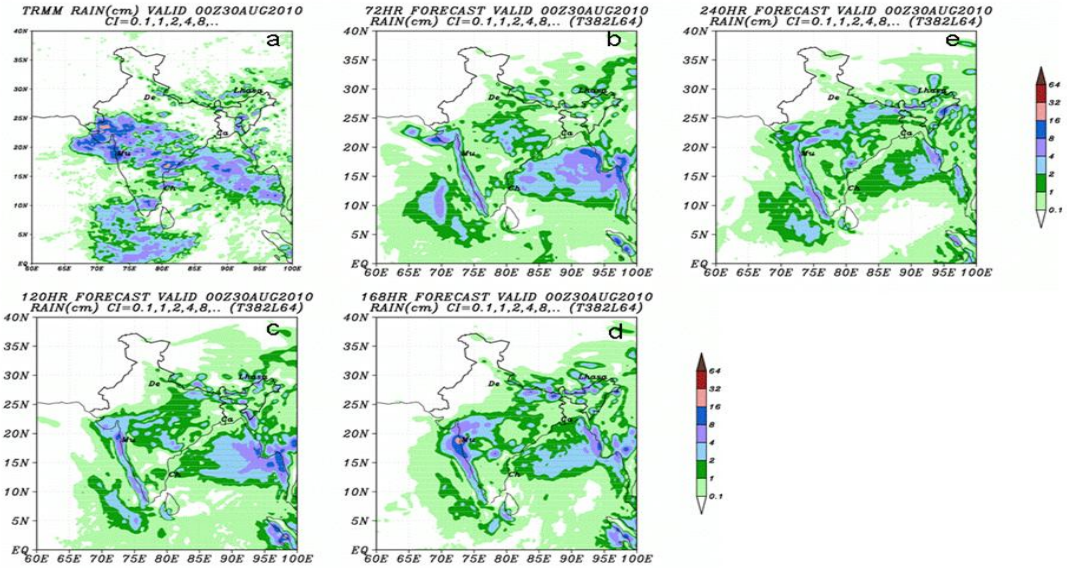

Fig. 7 Daily rainfall (cm/day) accumulated upto 00Z 30 August, 2010; (a) TRMM derived dataset (b) Day-3 forecast (c) Day-5 forecast (d) Day-7 and (e) Day-10 forecast from T382L64 system.

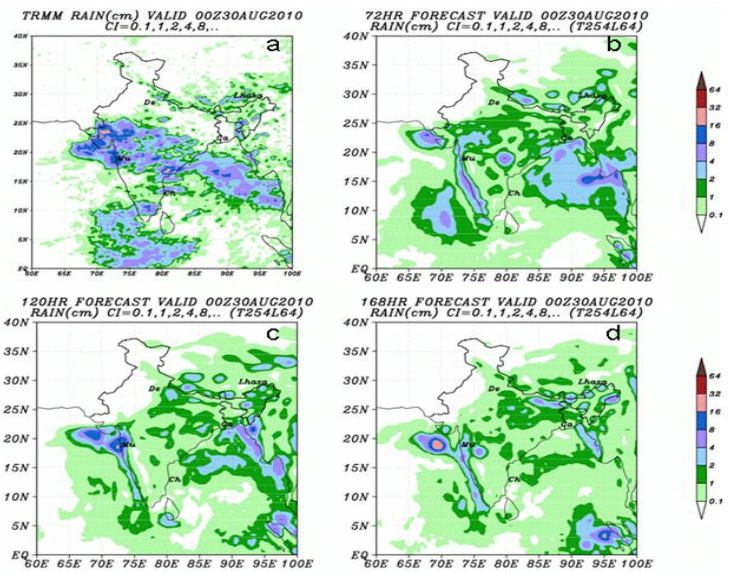

Fig. 8 Daily rainfall (cm/day) accumulated upto 00Z 30 August, 2010; (a) TRMM derived dataset (b) Day-3 forecast (c) Day-5 forecast and (d) Day-7 forecast from T254L64 system.

b. Tropical Cyclone Jal (6-7,November, 2010):

Similar analysis is done for the Tropical cyclone (TC) Jal. TC Jal developed from an LPA over South China Sea and developed in to tropical depression on 28 October. On 1 November, the system crossed over to southeast Bay of Bengal as tropical depression. Further the system showed slow westward movement and development, but degraded into a low. On 4 November, it was upgraded again to depression BOB 05 and on 5 Novemeber into Deep depression. On 6 November it developed into TC (Jal) and on 7 November, weakened fast, ultimately land falling at Chennai just before the dawn of 8 November.

Fig. 9 depicts the wind and geopotential valid for 00Z 0f 06 November 2010. T382L64 forecast of days 3, 5 and 7 are plotted against the verifying analysis from the same system. The day-3 forecast shows better match in intensity with the analysis whereas the Day-5 and Day-7 forecasts give slightly stronger system. Though the location of Day-5 forecast is slightly displaced near to the land, in general the system was predicted satisfactorily in all forecasts. Fig. 10 is the corresponding plot for T254L64 system. In general T254L64 analysis and day-3 show more intense system compared to T382L64. However, comparing the intensity and location, T254L64 shows less perfect match with the corresponding analysis compared to T382L64 system. In fact Day-3 forecast shows over intensification compared to the Day-5 or Day-7. In general T254L64 shows a tendency to over predict the intensity of the weather systems. Here also the Day-5 forecast is found to be more near to land.

The panels of associated rainfall (Figs. 11-12) show the impact of T382L64 and T254L64 runs on the rainfall forecasts. The rainfall intensity was more or less predicted by both models, but the location is better matching for T382L64 compared to T254L64 runs. T254L64 model tries to predict the location towards north of TRMM rainfall. Here also T382L64 is able to fairly well predict the system 10 days in advance.

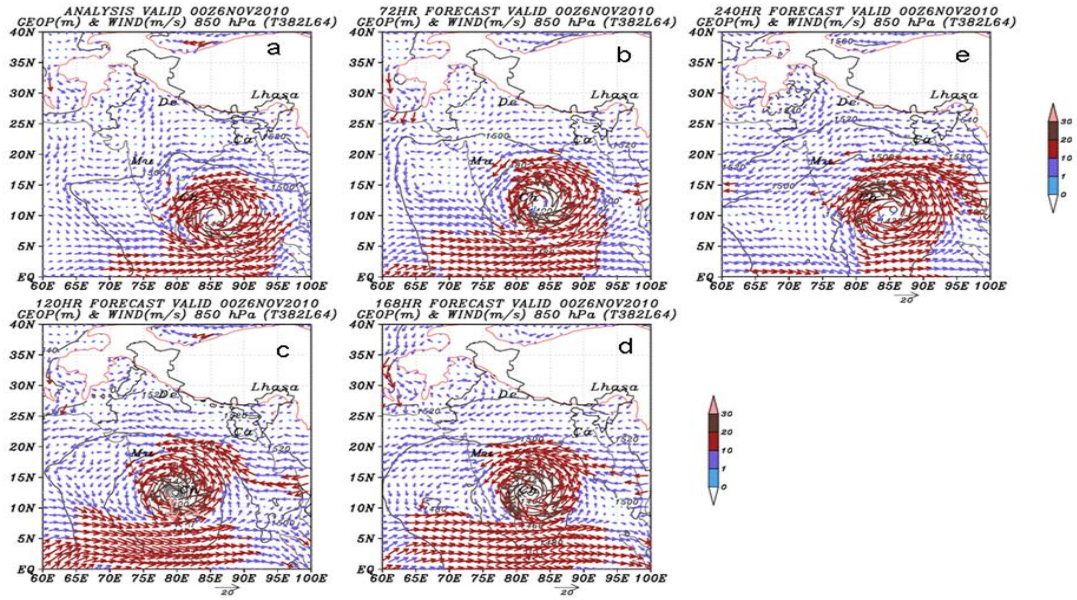

Fig. 9 Wind (m/s) and Geopotential (m) valid for 00Z 06 November, 2010; (a) analysis (b) Day-3 forecast (c) Day-5 forecast and (d) Day-7 forecast, all from T382L64 system.

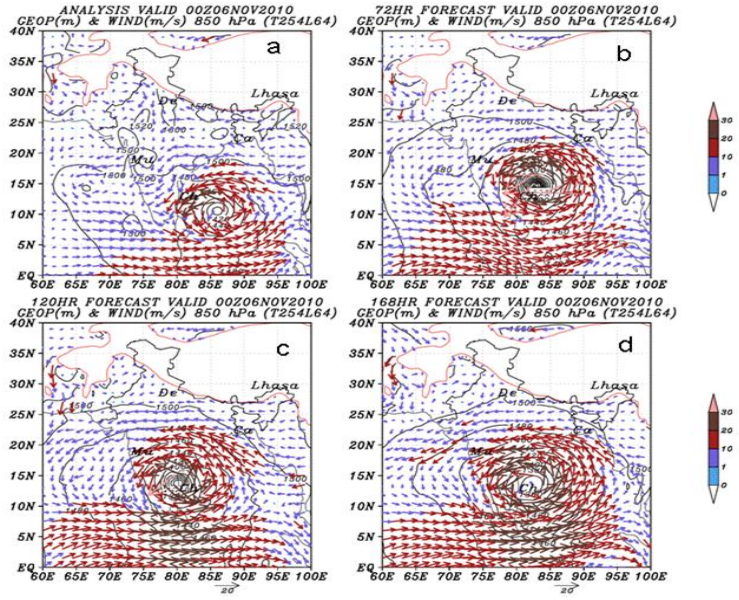

Fig. 10 Wind (m/s) and Geopotential (m) valid for 00Z 06 November, 2010; (a) analysis (b) Day-3 forecast (c) Day-5 forecast and (d) Day-7 forecast, all from T254L64 system.

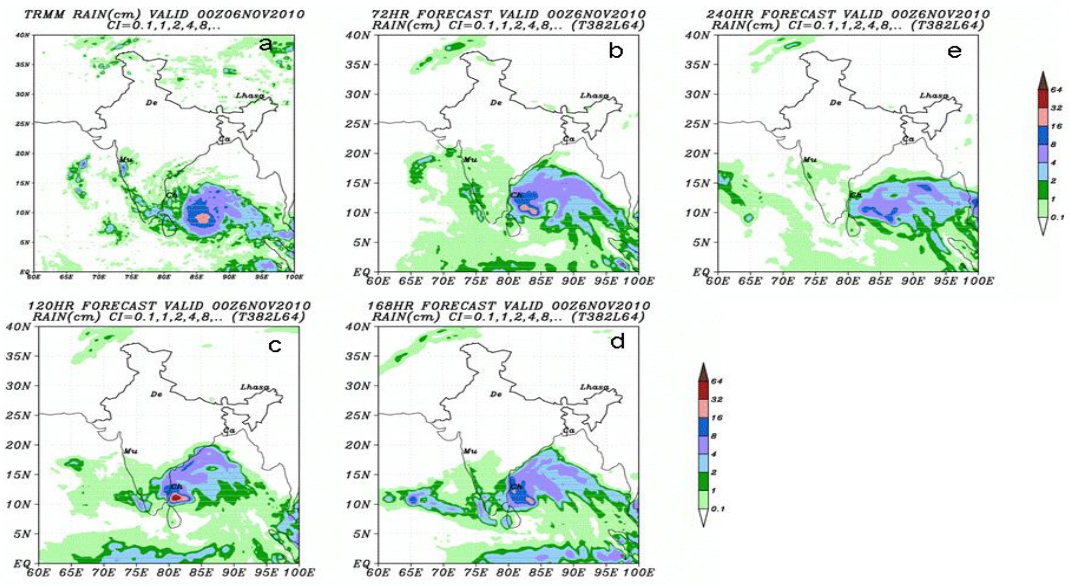

Fig. 11 Daily rainfall (cm/day) accumulated upto 00Z 06 November, 2010; (a) TRMM (b) Day-3 forecast (c) Day-5 forecast and (d) Day-7 forecast from T382L64 system.

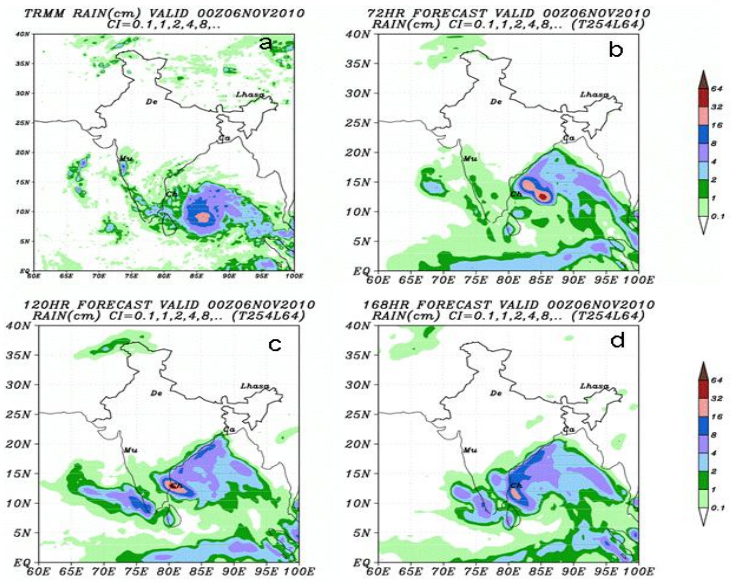

Fig. 12 Daily rainfall (cm/day) accumulated upto 00Z 06 November, 2010; (a) TRMM (b) Day-3 forecast (c) Day-5 forecast and (d) Day-7 forecast from T254L64 system.

7. Up-gradation and model resolutions

The new GFS system was upgraded in horizontal resolution from T382L64 to T574L64 and is run parallel from 15 November, 2010. T547L64 has 574 waves in the zonal direction with Triangular truncation, 64 vertical levels and a Gaussian grid of 1760x880 points. The reduced grid structure is given in Table 12. It has a resolution of around 23Km over the equator. It has a timestep of 120 seconds and takes around 15 minutes for 24 hour forecast in 16 nodes and 32 processors on IBM Power 6.

Table 12 The reduced grid structure of T574L64 from pole to equator over the 440 Gaussian latitudes.

---

18 28 32 42 48 56 64 72 80 84
90 110 110 110 120 126 132 140 144 154
160 168 176 176 192 192 198 210 210 220
224 240 240 252 252 256 264 280 280 288
288 308 308 308 320 320 330 330 352 352
352 360 384 384 384 384 396 396 420 420
420 420 440 440 440 448 462 462 462 480
480 480 504 504 504 504 512 528 528 528
560 560 560 560 560 576 576 576 616 616
616 616 616 616 630 630 630 640 660 660
660 660 672 672 704 704 704 704 704 720
720 720 768 768 768 768 768 768 768 768
770 792 792 792 792 840 840 840 840 840
840 840 840 880 880 880 880 880 880 880
896 896 896 896 924 924 924 924 924 960
960 960 960 960 960 960 990 990 990 990
990 1008 1008 1008 1008 1024 1024 1024 1056 1056
1056 1056 1056 1056 1120 1120 1120 1120 1120 1120

1120 1120 1120 1120 1120 1120 1120 1152 1152 1152
1152 1152 1152 1152 1232 1232 1232 1232 1232 1232
1232 1232 1232 1232 1232 1232 1232 1232 1232 1232
1232 1260 1260 1260 1260 1260 1260 1260 1280 1280
1280 1280 1280 1320 1320 1320 1320 1320 1320 1320
1320 1320 1344 1344 1344 1344 1344 1344 1386 1386
1386 1386 1386 1386 1386 1386 1386 1386 1386 1408
1408 1408 1408 1408 1440 1440 1440 1440 1440 1440
1440 1440 1440 1440 1536 1536 1536 1536 1536 1536
1536 1536 1536 1536 1536 1536 1536 1536 1536 1536
1536 1536 1536 1536 1536 1536 1536 1536 1536 1536
1536 1536 1536 1536 1584 1584 1584 1584 1584 1584
1584 1584 1584 1584 1584 1584 1584 1584 1584 1584
1584 1680 1680 1680 1680 1680 1680 1680 1680 1680
1680 1680 1680 1680 1680 1680 1680 1680 1680 1680
1680 1680 1680 1680 1680 1680 1680 1680 1680 1680
1680 1680 1680 1680 1680 1680 1680 1680 1680 1680
1680 1680 1680 1680 1680 1680 1680 1680 1760 1760
1760 1760 1760 1760 1760 1760 1760 1760 1760 1760
1760 1760 1760 1760 1760 1760 1760 1760 1760 1760
1760 1760 1760 1760 1760 1760 1760 1760 1760 1760
1760 1760 1760 1760 1760 1760 1760 1760 1760 1760
1760 1760 1760 1760 1760 1760 1760 1760 1760 1760
1760 1760 1760 1760 1760 1760 1760 1760 1760 1760
1760 1760 1760 1760 1760 1760 1760 1760 1760 1760

The post processing is done in Gaussian grids either with POSTGP or with NCEPPOST, but can be converted to any regular grid resolution grib output using COPYGB utility. For tropical cyclone relocation, the post processing is done at 0.5 degree resolution (either with

POSTGP directly or with NCEPPOST and COPYGB utilities). Major problem with the upgradation was the AIX memory allocation to handle the huge file size being read in. This was solved by adopting AIX Large Memory Model and by inserting the following export statement in the Job;

'export LDR_CNTRL=MAXDATA=0x8000000000'.

The T574L64 implementation employed the full range of new physics options. The differences in the namelist options for T574L64 model from those listed in Section (4b) are listed below:

DELTIM=120.0,	Time-step
FHLWR=1.0,	LW radiation calling interval is 1 hour
OUT_VIRTTEMP=F,	(No effect for this option)
JCAP=574,	Spectral truncation
LONF=1760,	Number of Gaussian longitudes
LONR=1760,	Number of Gaussian longitudes
LATG=880,	Number of Gaussian latitudes
LATR=880,	Number of Gaussian latitudes
ICO2=1,	Observed CO2 global annual mean value
IAER=111,	Volcanic (stratospheric) and tropospheric aerosol effect for LW and SW
OLD_MONIN=F,	New PBL scheme used
SASHAL=T,	New mass-flux shallow convection used
NEWSAS=T,	New SAS convection used
ZFLXTVD=T,	Positive-definite tracer transport (flux-limited vertical advection) used
TRANS_TRAC=F,	(Used only for RAS)

8. Model performance Inter-comparisons

The comparison of the three GFS systems, namely, T254L64, T382L64 and T574L64 and is carried out in this section. The major differences in the three systems are mentioned in the previous sections. An idea of the major differences between T382L64 and T574L64 physics options can be obtained by referring to the sections 4d and 7. The T382L64 physics is closer to T254L64 as the namelist options of specifying modified physics schemes were not used in T382L64 runs thus taking old physics by default. The comparison of the three models were

carried out for one Western Disturbance (WD) and one Easterly Wave (EW) cases during the winter season of 2010-11, immediately following the implementation of T574L64 system in November 2010. These cases are (i) EW (1-2 February, 2011) and (ii) WD (7-8 February, 2011) in which the comparatively weak rain was mainly concentrated over 1-2 days period over the northwest India including Delhi and over the southern peninsula, respectively.

a. Case studies:

EW (02 February 2011): The figures 13-18 displays the model forecasts compared with the analysis or TRMM rainfall estimates. T574L64 is able to fairly well predict the easterly wave 3 days in advance in intensity as well as location. Rainfall is well matching in the quantity and spread upto day-3, and thereafter the spread is drastically reduced. For T382L64 and T254L64 models, the analyses shows more intense system, and is predicted 3 days in advance with some minor differences in the location and spread. Beyond Day-3, both T382L64 and T254L64 show more displacement away from the analysis with the activities concentrated elsewhere from the actual location. There is an anomalous second system seen in T382L64 forecasts in these forecast time ranges, towards east of the original system. T574L64 does not predict these anomalous formations. T254L64 predicts the EW system up to 7 days in advance but with an apparent slower westward speed and thus located eastward of the analysis position, which is also reflected in the displaced rainfall patterns. In general, from the rainfall predictions, it can be clearly seen that T574L64 prediction is superior to T382L64 or T254L64 predictions. However, T574L64 shows reduced activity and signal at the longer time ranges in this particular case for the relatively weaker synoptic systems over the equatorial latitudes. A prediction of a strong synoptic system like tropical cyclone could not be attempted during the experimental period due to the lack of such cases during these couple of months.

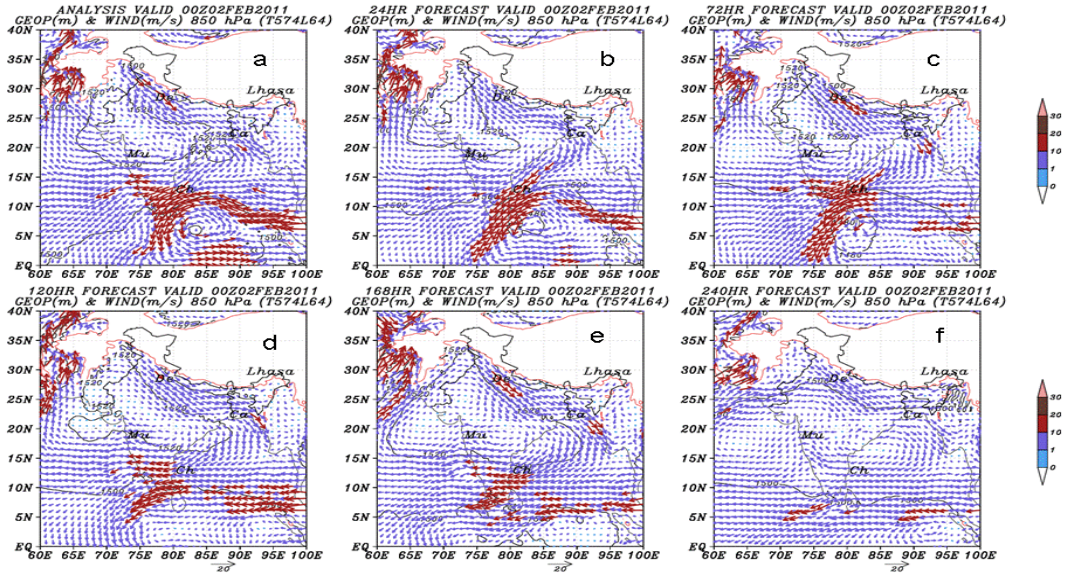

Fig. 13 850hPa wind vectors (m/s) and geopotemtial (m) for analysis (a) 24-hr forecast (b) 72-hr forecast (c) 120-hr forecast (d) 168-hr forecast (e) and 240-hr forecast (f) by T574L64 model, valid for 02 February, 2011.

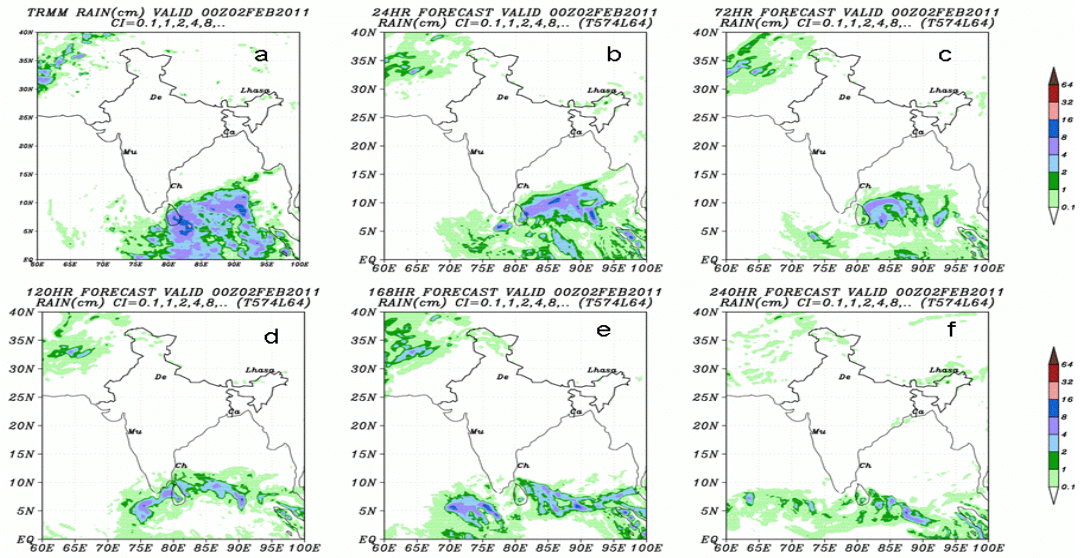

Fig. 14 Similar to Fig. 13, but for daily rainfall (cm/day). The panel (a) shows the TRMM derived daily rainfall valid for 00Z , 02 February, 2011.

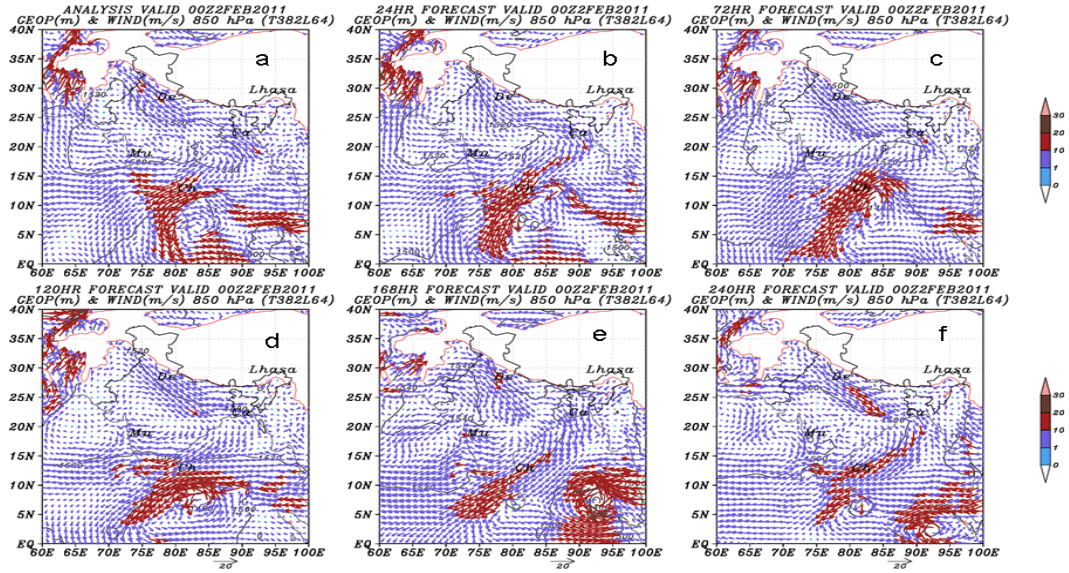

Fig. 15 Similar to Fig. 13, but for T382L64 model.

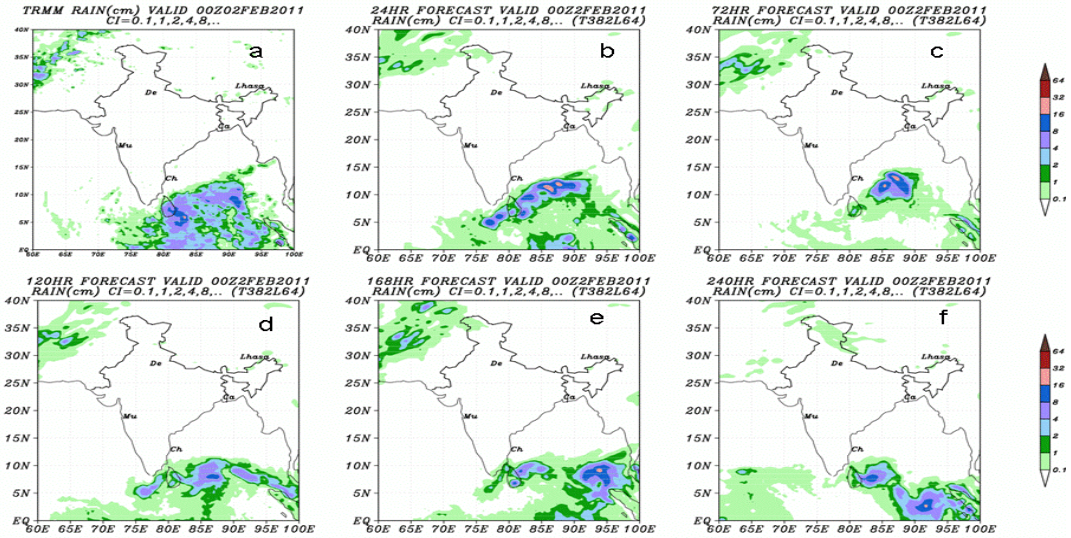

Fig. 16. Similar to Fig. 14, but for T382L64 model.

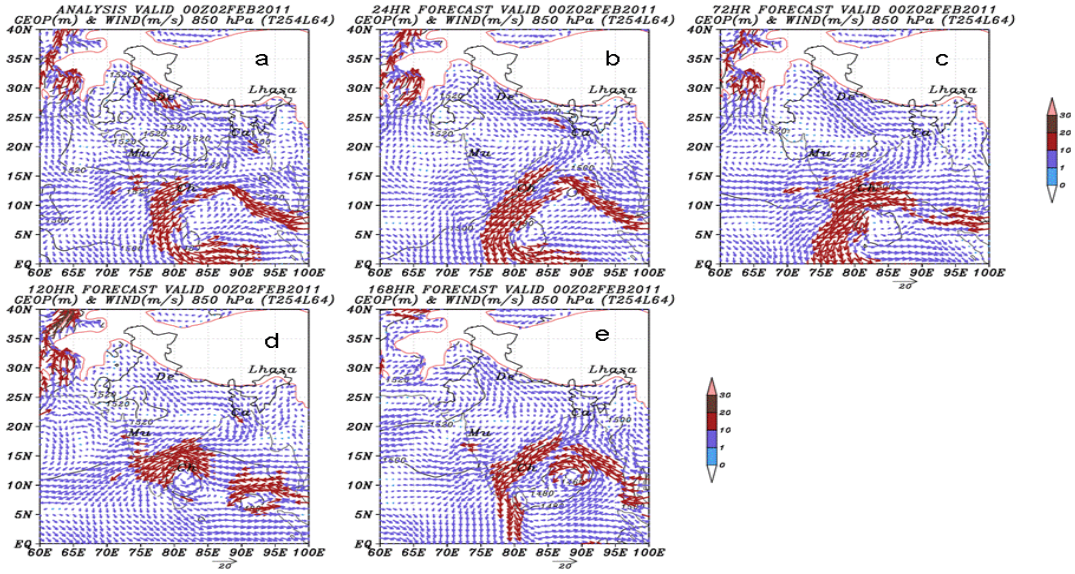

Fig. 17 Similar to Fig. 13, but for T254L64 model.

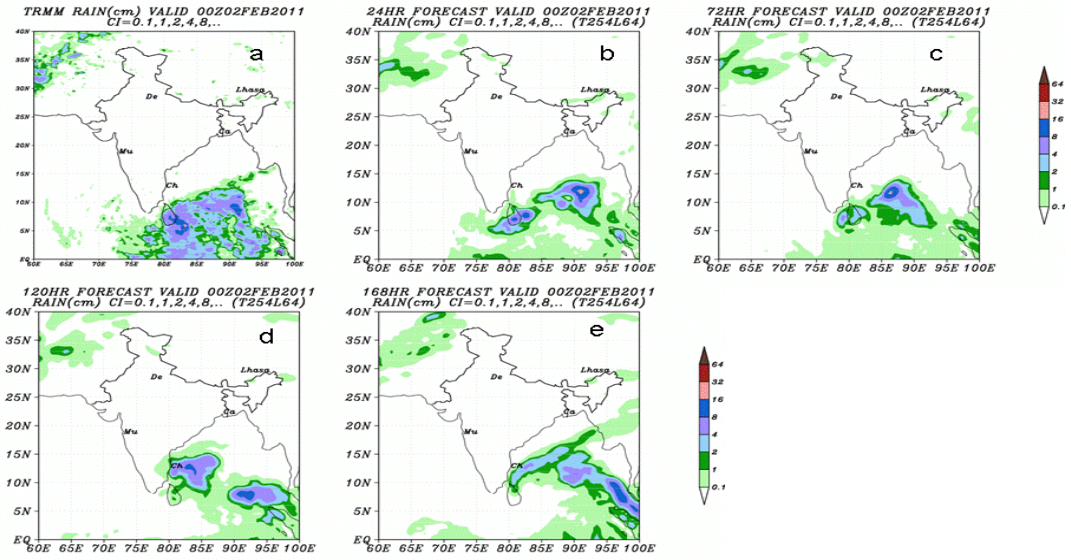

Fig. 18 Similar to Fig. 14, but for T254L64 model.

WD (08 February 2011): The figures 19-24 depicts the prediction of WD for the three models in terms of wind, geopotential and rainfall. All the three models predicted the westerly trough fairly well upto Day-3. Day-5 prediction shows slightly slow propagation of the WD and at Day-7, the trough is not as strong as seen in the analysis in the case of

T574L64 and T382L64. Day-7 prediction by T254L64 shows no trough in the vicinity of Jammu and Kashmir, thus gravely under predicting the eastward propagation speed of the westerly trough. Thus the Day-7 prediction of WD is better in the new models compared to T254L64 in this case. Between the two new models, the Day-10 prediction of the westerly trough is superior in T574L64 compared to T382L64 in terms of the intensity, while the location is again over the west of that in the analysis. The impact on the associated rainfall is clearly seen in the figures. Upto Day-3 the associated rainfall is fairly well predicted and comparable in T574L64 and T382L64 runs and is having a slight positive edge over the T254L64 prediction. The Day-5 pattern is also reasonably well predicted by all the three. However, the Day-10 prediction is better in T574L64 compared to T382L64 as far as the rainfall activity is concerned.

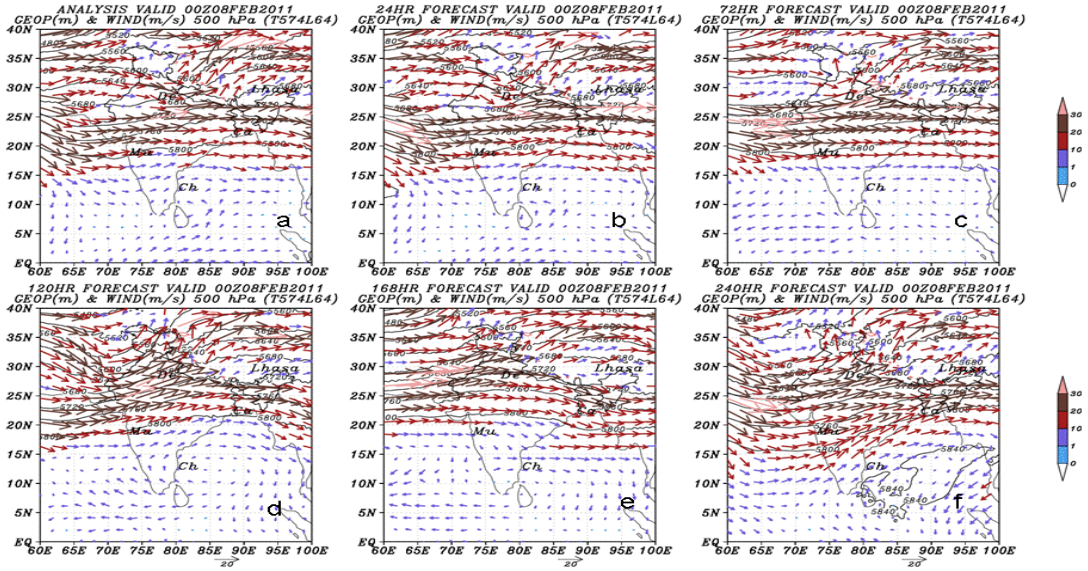

Fig. 19 500hPa wind vectors (m/s) and geopotemtial (m) for analysis (a) 24-hr forecast (b) 72-hr forecast (c) 120-hr forecast (d) 168-hr forecast (e) and 240-hr forecast (f) by T574L64 model, valid for 08 February, 2011.

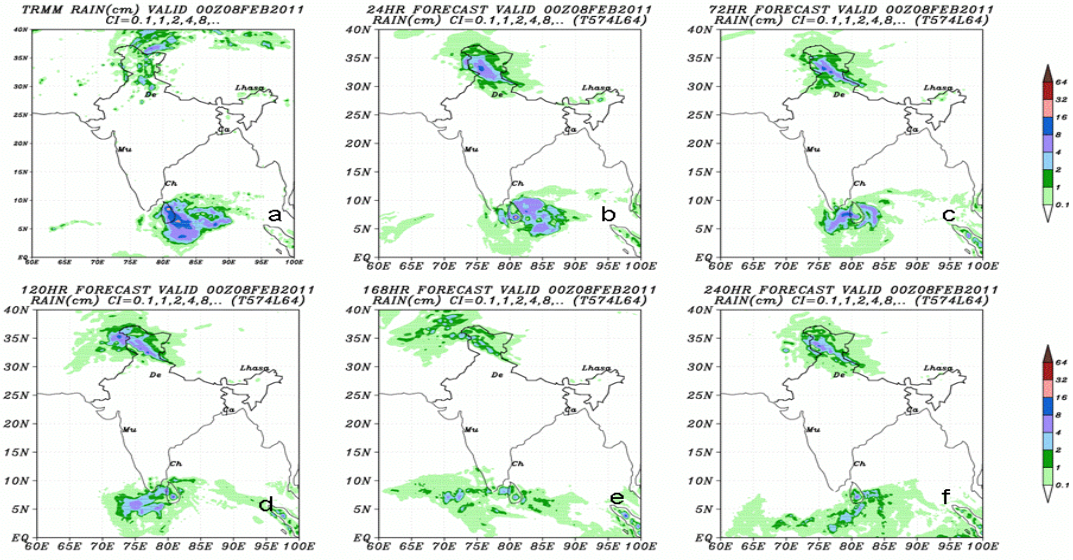

Fig. 20 Similar to Fig. 19, but for daily rainfall (cm/day). The panel (a) shows the TRMM derived daily rainfall valid for 00Z, 08 February, 2011.

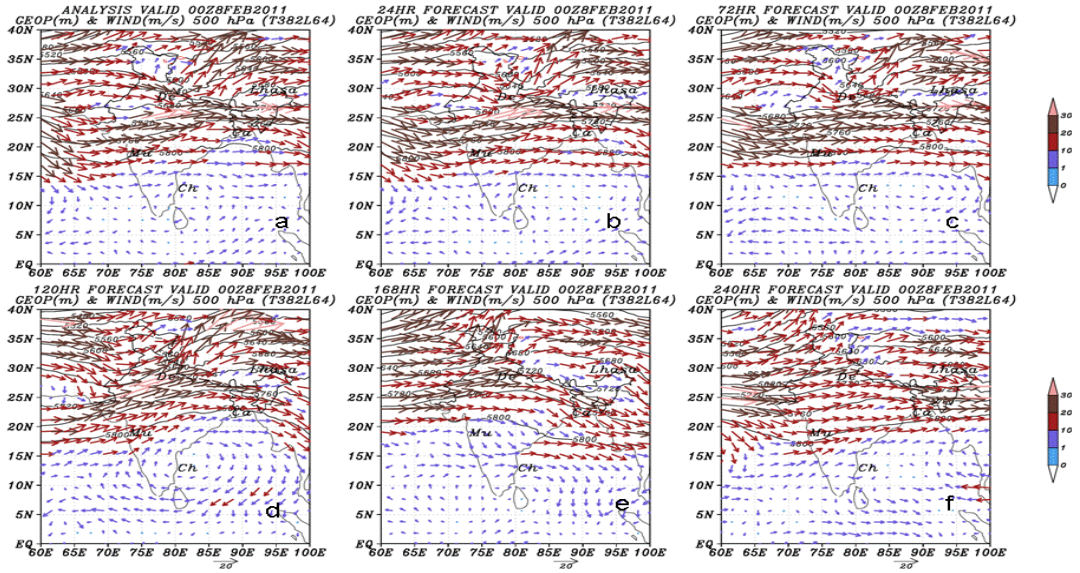

Fig. 21 Similar to Fig. 19, but for T382L64 model.

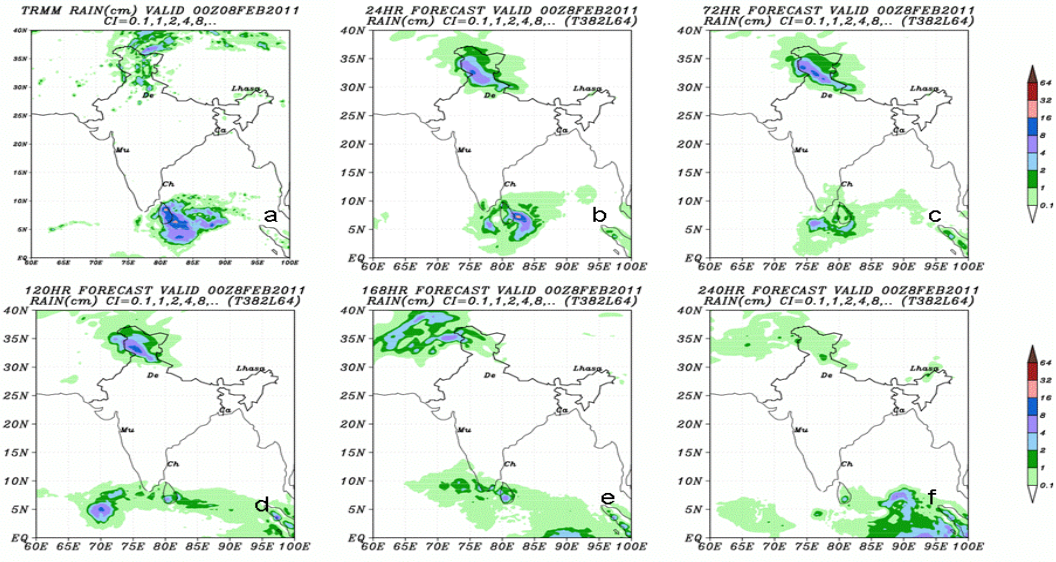

Fig. 22 Similar to Fig. 20, but for T382L64 model.

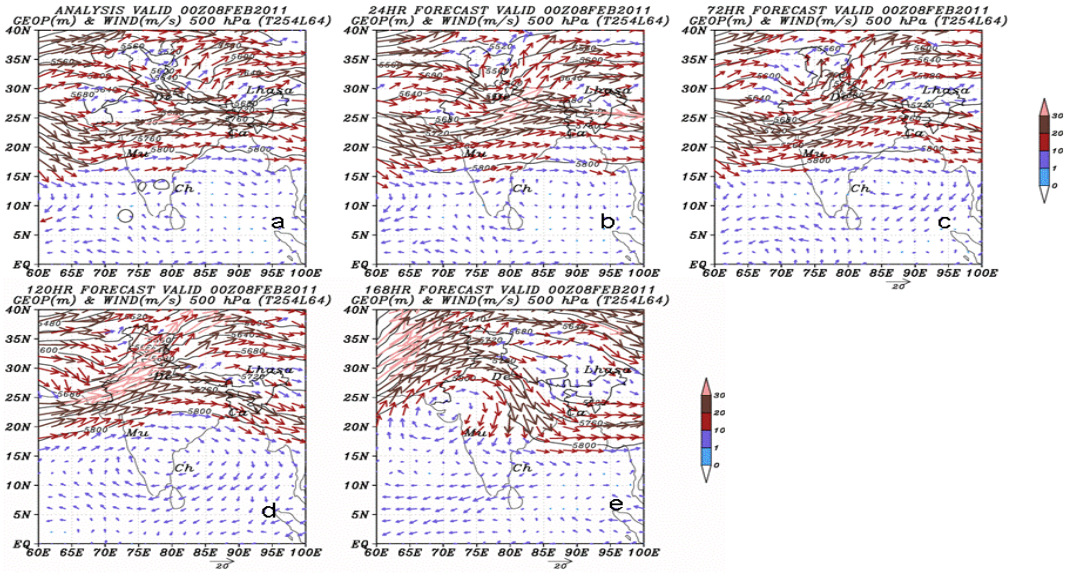

Fig. 23 Similar to Fig. 19, but for T254L64 model.

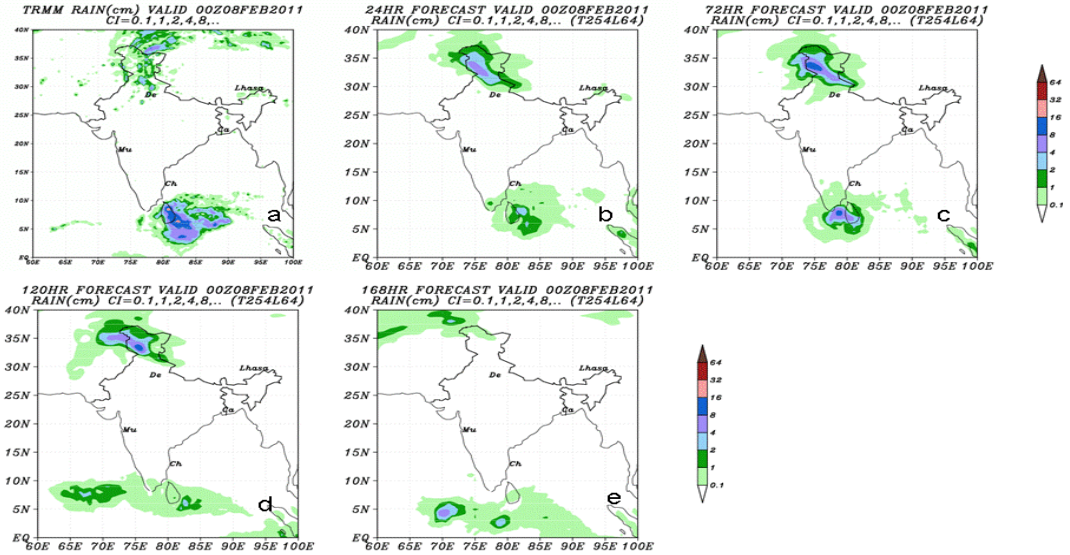

Fig. 24 Similar to Fig. 20, but for T254L64 model.

b. Model verification scores

The study region has been divided into five sections: G2-Globe, NHX-Northern Hemisphere (20^0N-80^0N), SHX-Southern Hemisphere (20^0S-80^0S), TRO-Tropics (20^0S-20^0N) and RSMC-India and surrounding region (20^0S-45^0N, 30^0E-120^0E). The performance of the T254L64, T382L64 and T574L64 model forecasts is investigated in terms of the mean analyses obtained from the three systems of experiments using the aforesaid models for the period 1st-10th April, 2011. Parameters such as geo-potential height, temperature and vector wind are analyzed.

Anomaly Correlation (AC): Figures 25, 26 & 27 presents the anomaly correlation for the temperature, vector wind and geo-potential height at 500hPa pressure level, respectively over (a) Globe, (b) Tropics, (c) Northern Hemisphere & (d) Southern Hemisphere. It is clearly seen that the T382L64 and T574L64 has higher anomaly correlation compared to that of T254L64, for almost all the regions over all the days of forecast. In the lower part of the figures, the difference of T382L64 and T574L64 anomaly correlation with respect to T254L64 is presented. The anomaly correlation differences outside the histograms are statistically significant at 95% level

of significance. The red line denotes the difference for T382L64 and the green line stands for T574L64. The temperature and vector wind AC over globe and tropics for T574L64 is significantly higher to T254L64 compared to that of T382L64; the difference being statistically significant at 95% level of significance in majority of cases. Over northern hemisphere, T574L64 has the best temperature, vector wind and geopotential height AC. The performance with respect to geopotential height AC for T382L64 and T574L64 is mixed. The similar mixed performance of T382L64 and T574L64 is obtained over RSMC region (Figure 28) for all the three parameters at 500hPa pressure level. Tables 13(a, b, c), 14(a, b, c) and 15(a, b, c) tabulates the anomaly correlation over Globe, NHX, SHX and RSMC (Tropics has not been included) for temperature and vector wind at 850, 500 and 250hPa and for geo-potential height at 700, 500 and 250hPa, respectively. The box representing the highest value in the group is shaded. In majority of cases T574L64 is scoring above T382L64 and T254L64. At 850hPa over RSMC region T382L64 has higher temperature and vector wind AC than the other two. For geopotential height AC, T382L64 is best over RSMC region.

	Table: 13a **Temperature Anomaly Correlation - Day-1 Forecast**											
Level hPa	***Global***			***N.H.X***			***S.H.X***			***RSMC***		
	T254	**T382**	**T574**	**T254**	**T382**	**T574**	**T254**	**T382**	**T574**	**T254**	**T382**	**T574**
850	0.959	0.968	0.960	0.969	0.974	0.972	0.954	0.968	0.958	0.922	0.948	0.938
500	0.969	0.977	0.978	0.982	0.985	0.986	0.961	0.976	0.977	0.919	0.935	0.936
250	0.945	0.968	0.970	0.969	0.975	0.978	0.915	0.961	0.962	0.913	0.957	0.955

	Table: 13b **Temperature Anomaly Correlation - Day-3 Forecast**											
Level hPa	***Global***			***N.H.X***			***S.H.X***			***RSMC***		
	T254	**T382**	**T574**	**T254**	**T382**	**T574**	**T254**	**T382**	**T574**	**T254**	**T382**	**T574**
850	0.872	0.906	0.898	0.909	0.921	0.926	0.836	0.894	0.881	0.876	0.900	0.891
500	0.868	0.901	0.904	0.917	0.929	0.933	0.822	0.879	0.880	0.808	0.845	0.861
250	0.815	0.864	0.877	0.874	0.892	0.911	0.706	0.809	0.812	0.803	0.885	0.891

	Table: 13c **Temperature Anomaly Correlation - Day-5 Forecast**											
Level hPa	***Global***			***N.H.X***			***S.H.X***			***RSMC***		
	T254	**T382**	**T574**	**T254**	**T382**	**T574**	**T254**	**T382**	**T574**	**T254**	**T382**	**T574**
850	0.703	0.766	0.767	0.768	0.792	0.815	0.633	0.735	0.729	0.781	0.820	0.811
500	0.676	0.733	0.755	0.762	0.784	0.822	0.588	0.679	0.676	0.648	0.692	0.728
250	0.647	0.703	0.727	0.734	0.760	0.804	0.449	0.586	0.579	0.660	0.835	0.784

	Table: 14a **Vector Wind Anomaly Correlation - Day-1 Forecast**											
Level hPa	***Global***			***N.H.X***			***S.H.X***			***RSMC***		
	T254	**T382**	**T574**	**T254**	**T382**	**T574**	**T254**	**T382**	**T574**	**T254**	**T382**	**T574**
850	0.931	0.943	0.946	0.948	0.952	0.954	0.934	0.949	0.954	0.855	0.890	0.887
500	0.952	0.959	0.962	0.965	0.965	0.967	0.953	0.963	0.965	0.891	0.907	0.918
250	0.953	0.966	0.968	0.969	0.972	0.975	0.958	0.973	0.974	0.910	0.929	0.933

	Table: 14b **Vector Wind Anomaly Correlation - Day-3 Forecast**											
Level hPa	***Global***			***N.H.X***			***S.H.X***			***RSMC***		
	T254	**T382**	**T574**	**T254**	**T382**	**T574**	**T254**	**T382**	**T574**	**T254**	**T382**	**T574**
850	0.784	0.830	0.833	0.850	0.852	0.869	0.739	0.823	0.817	0.741	0.806	0.777
500	0.825	0.865	0.869	0.878	0.882	0.892	0.797	0.861	0.856	0.751	0.797	0.810
250	0.828	0.879	0.886	0.890	0.903	0.910	0.810	0.881	0.884	0.803	0.839	0.847

	Table: 14c **Vector Wind Anomaly Correlation - Day-5 Forecast**											
Level hPa	***Global***			***N.H.X***			***S.H.X***			***RSMC***		
	T254	**T382**	**T574**	**T254**	**T382**	**T574**	**T254**	**T382**	**T574**	**T254**	**T382**	**T574**
850	0.550	0.624	0.639	0.641	0.656	0.699	0.474	0.584	0.590	0.564	0.679	0.616
500	0.593	0.671	0.691	0.682	0.702	0.745	0.529	0.647	0.648	0.574	0.649	0.616
250	0.617	0.704	0.729	0.719	0.743	0.786	0.566	0.693	0.698	0.644	0.732	0.702

	Table: 15a **Geo-potential Height Anomaly Correlation - Day-1 Forecast**											
Level hPa	***Global***			***N.H.X***			***S.H.X***			***RSMC***		
	T254	**T382**	**T574**	**T254**	**T382**	**T574**	**T254**	**T382**	**T574**	**T254**	**T382**	**T574**
700	0.987	0.993	0.993	0.993	0.995	0.995	0.982	0.991	0.991	0.956	0.976	0.973
500	0.989	0.994	0.994	0.994	0.996	0.996	0.985	0.993	0.993	0.973	0.984	0.980
250	0.989	0.995	0.995	0.994	0.996	0.996	0.986	0.994	0.994	0.973	0.987	0.986

	Table: 15b **Geo-potential Height Anomaly Correlation - Day-3 Forecast**											
Level hPa	***Global***			***N.H.X***			***S.H.X***			***RSMC***		
	T254	**T382**	**T574**	**T254**	**T382**	**T574**	**T254**	**T382**	**T574**	**T254**	**T382**	**T574**
700	0.912	0.952	0.952	0.951	0.964	0.968	0.867	0.938	0.932	0.873	0.922	0.911
500	0.920	0.956	0.954	0.956	0.968	0.970	0.882	0.943	0.938	0.892	0.922	0.913
250	0.926	0.961	0.961	0.961	0.972	0.973	0.892	0.948	0.948	0.901	0.943	0.943

	Table: 15c **Geo-potential Height Anomaly Correlation - Day-5 Forecast**											
Level hPa	***Global***			***N.H.X***			***S.H.X***			***RSMC***		
	T254	**T382**	**T574**	**T254**	**T382**	**T574**	**T254**	**T382**	**T574**	**T254**	**T382**	**T574**
700	0.733	0.809	0.821	0.818	0.855	0.881	0.636	0.743	0.749	0.724	0.829	0.810
500	0.741	0.818	0.829	0.831	0.867	0.888	0.651	0.760	0.767	0.708	0.814	0.796
250	0.765	0.840	0.853	0.854	0.882	0.903	0.676	0.788	0.795	0.714	0.831	0.825

Pattern Correlation (PC): Similar to anomaly correlation, in majority of cases the pattern correlation values are found to be lowest for T254L64 and highest for T574L64 at both upper and lower layers for all the regions (figures not shown). The values of T382L64 and T574L64 vector wind PC are close to each other over RSMC and southern hemisphere at both upper and lower levels (figures not shown) but over northern hemisphere T574L64 vector wind PC is higher to that of T382L64. Over globe, tropics and RSMC region, the T574L64 has mostly higher PC values for temperature at 500hPa (figure 29) compared to T382L64. At 200hPa (figure 30) both T382L64 and T574L64 has mixed performance. The quantitative difference of T574L64 temperature PC values from T254L64 is higher and statistically of more significance than that those of T382L64 at 500hPa pressure level.

Root Mean Square Error (RMSE): Like anomaly and pattern correlation, the performance of T382L64 and T574L64 is in edge over T254L64 in terms of root mean square error. In majority of cases, the RMSE of T574L64 is the lowest. The vector wind RMSE values of T574L64 over globe, northern hemisphere and tropics are lower compared to T382L64 (figures not shown). Over southern hemisphere the results are mixed. At both 500 and 200hPa, temperature RMSE values (figure 31 & 32, respectively) of T574L64 are significantly lower to that of T382L64. With the advance in forecast days, there is quantitative increase in the differences in RMSE of T574L64 with respect to the other two models. Also for geo-potential height (figures not shown), among the three models T574L64 has the lowest RMSE values over globe and northern hemisphere, the differences with respect to T254L64 being statistically and quantitatively significant compared to that of T382L64. Over other regions, the geopotential height rmse values are mixed. Over RSMC region, the vector wind RMSE values of T382L64 and T574L64 are close to each other at both 500 (figure 33c) and 200hPa (figure 33d) pressure levels. But, at 500 and 200hPa temperature RMSE values (figure 33a & 33b, respectively) of T574L64 are significantly lower.

9. Summary

The upgraded GFS systems were implemented on IBM-P6 systems at NCMRWF in two horizontal resolutions - T382 and T574 and 64 hybrid levels in the vertical. A new file structure was designed within a root directory of 'gfs' with a focus on the easy migration of the modelling system between the user accounts or across the machines. There is a major jump in the volume of satellite observations being assimilated in the new system and there is a change in the bufr decoders. T382L64 model is a replacement of the T254L64 model on the new HPC with some minor modification in the physics. However, T574L64 contains major modification in the model physics as per the status of NCEP version uploaded on 28 July, 2010.

T382L64 model has been running continuously from May, 2010 and T574L64 from November, 2010 for a couple of months. The comparison of the model statistics reveals that both T382L64 and T574L64 performances are superior to T254L64 system.

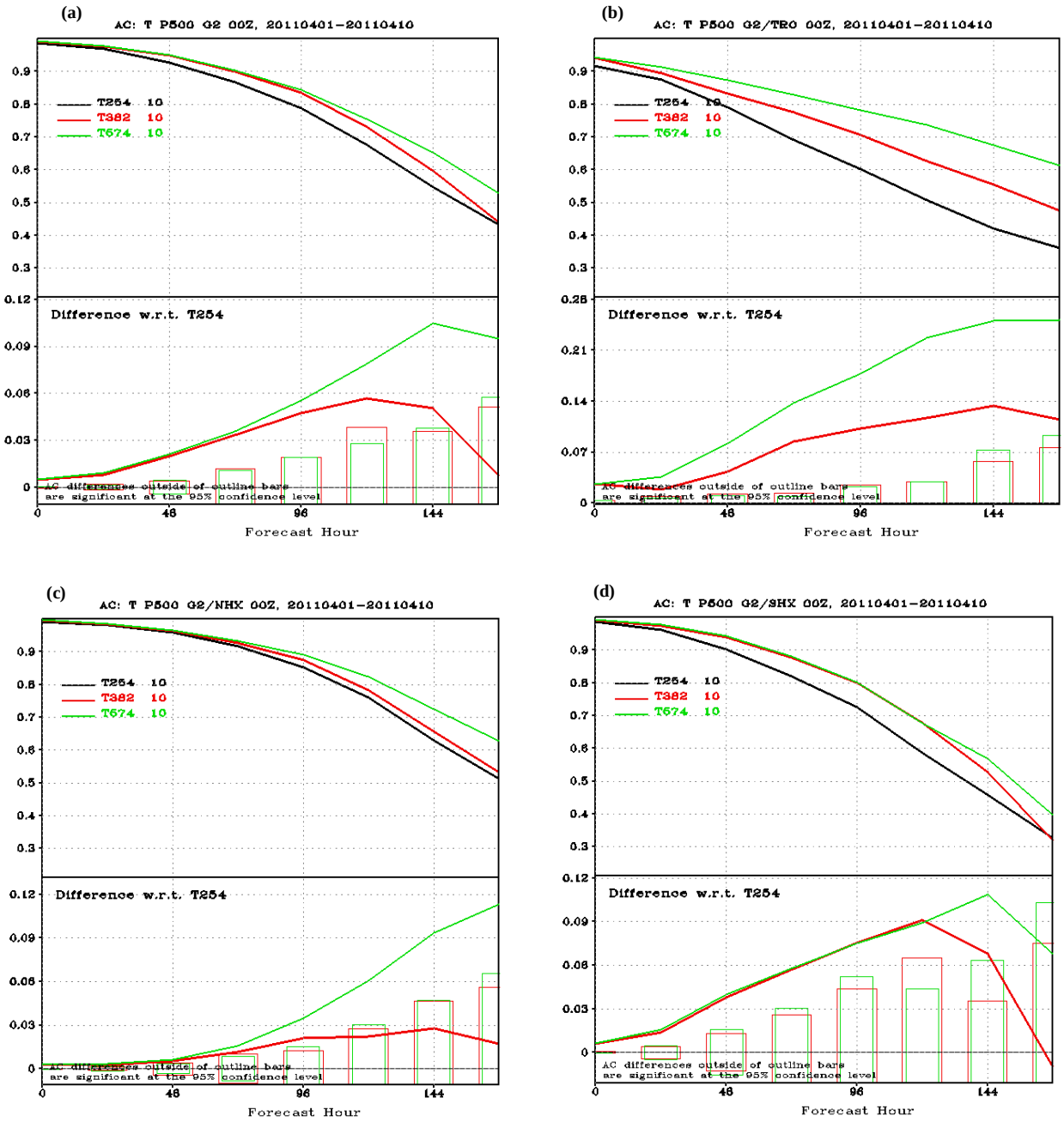

Figure 25: Anomaly Correlation (AC) of Temperature at 500hPa (upper part) and difference of Mean (AC) w.r.t T254L64 and its statistical significance (lower part) for (a) Globe, (b) Tropics, (c) Northern Hemisphere and (d) Southern Hemisphere.

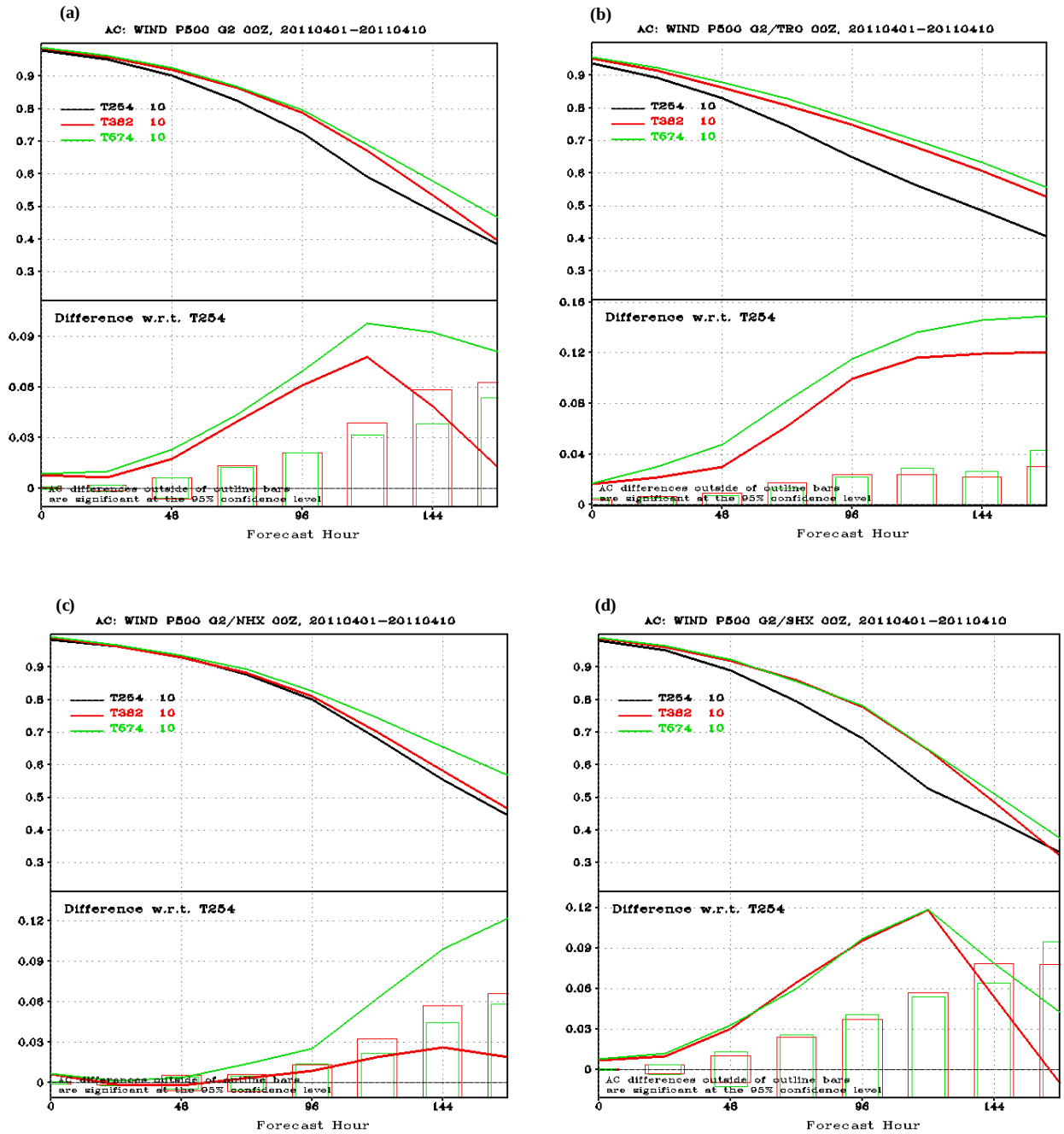

Figure 26: Same as figure 25 but for Horizontal Wind.

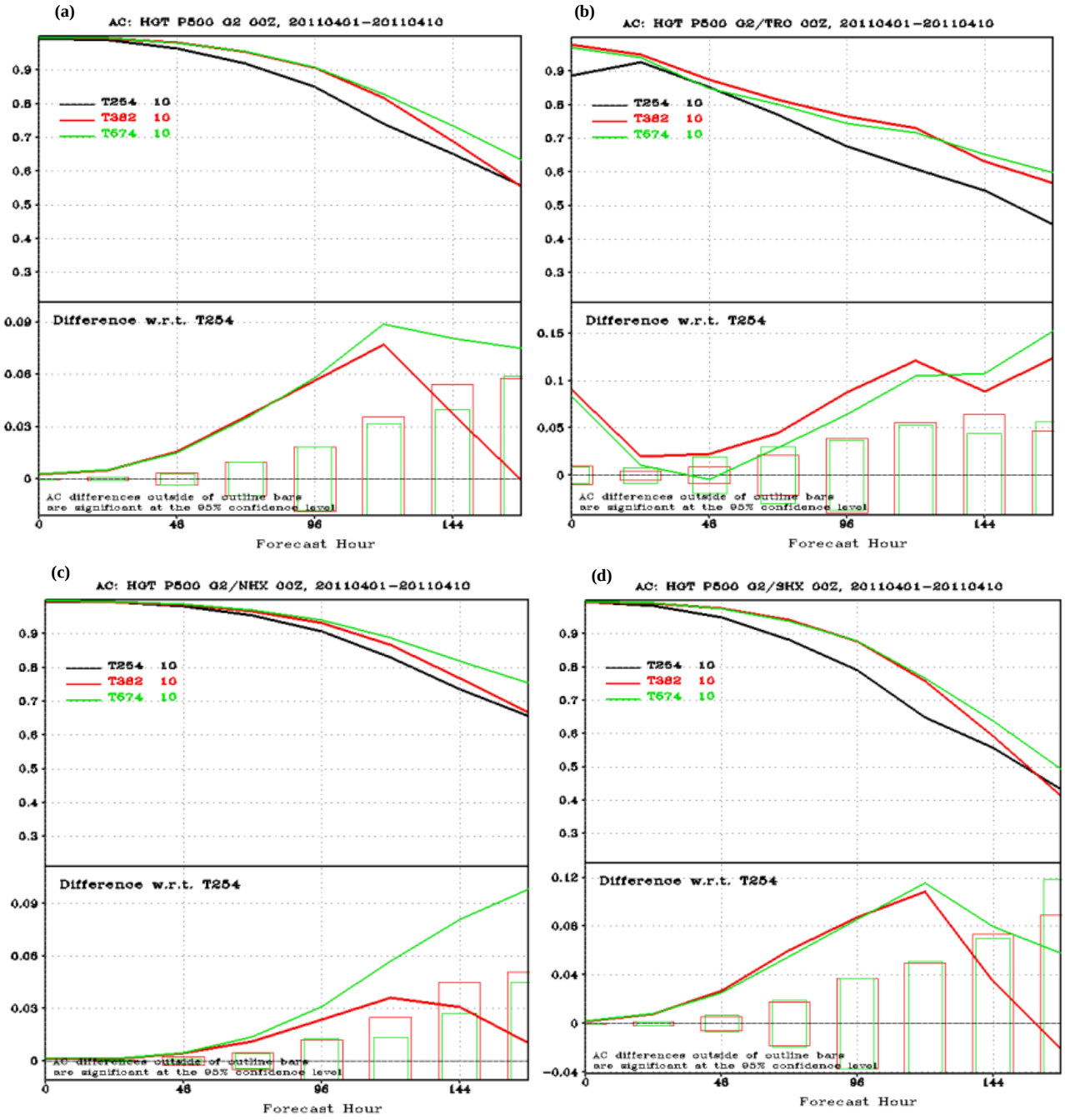

Figure 27: Same as figure 25 but for Geo-Potential Height.

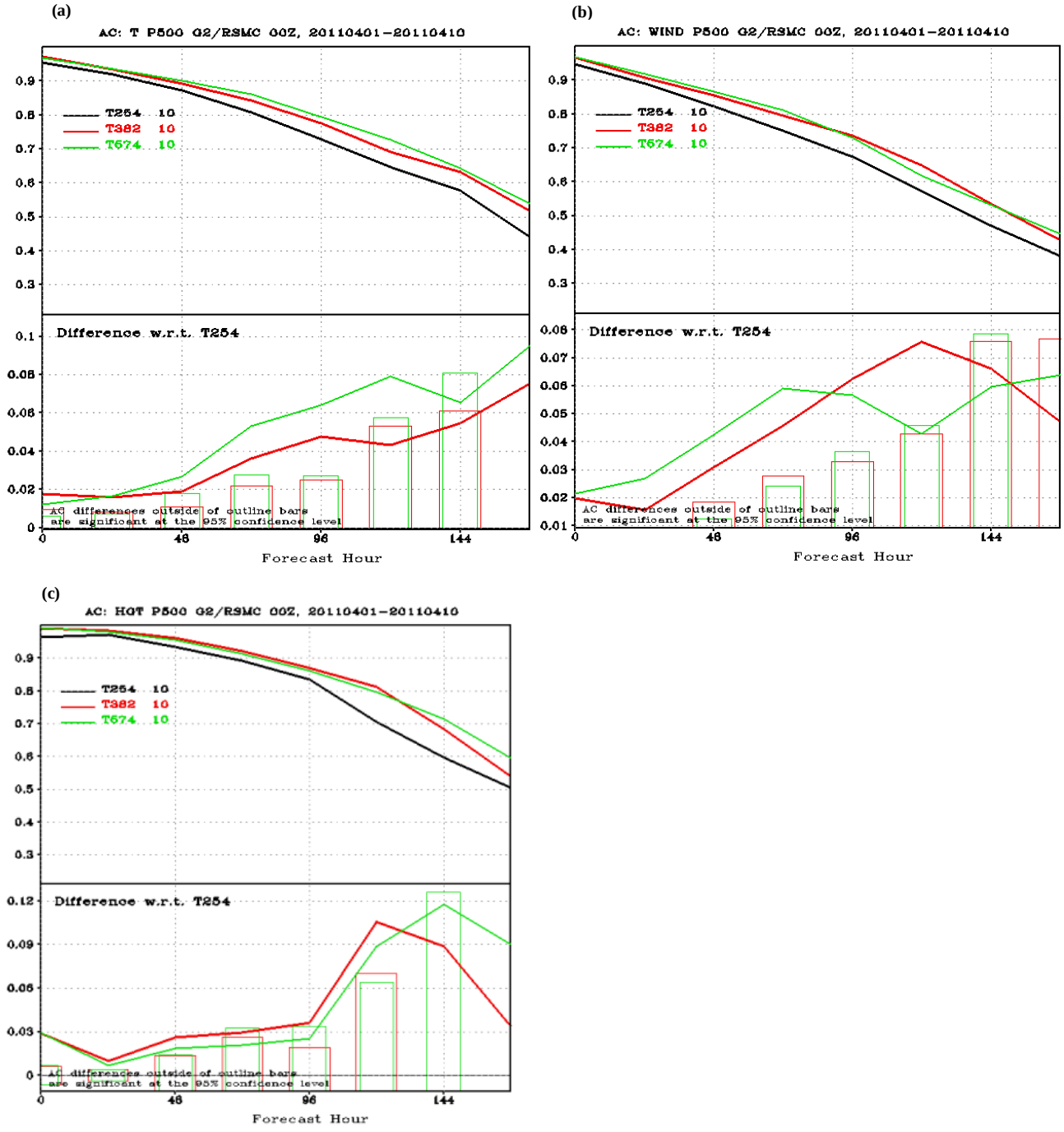

Figure 28: Anomaly Correlation (AC) at 500hPa over RSMC region (upper part) and difference of Mean (AC) w.r.to T254L64 and its statistical significance (lower part) for (a) Temperature, (b) Vector Wind, and (c) Geo-Potential Height.

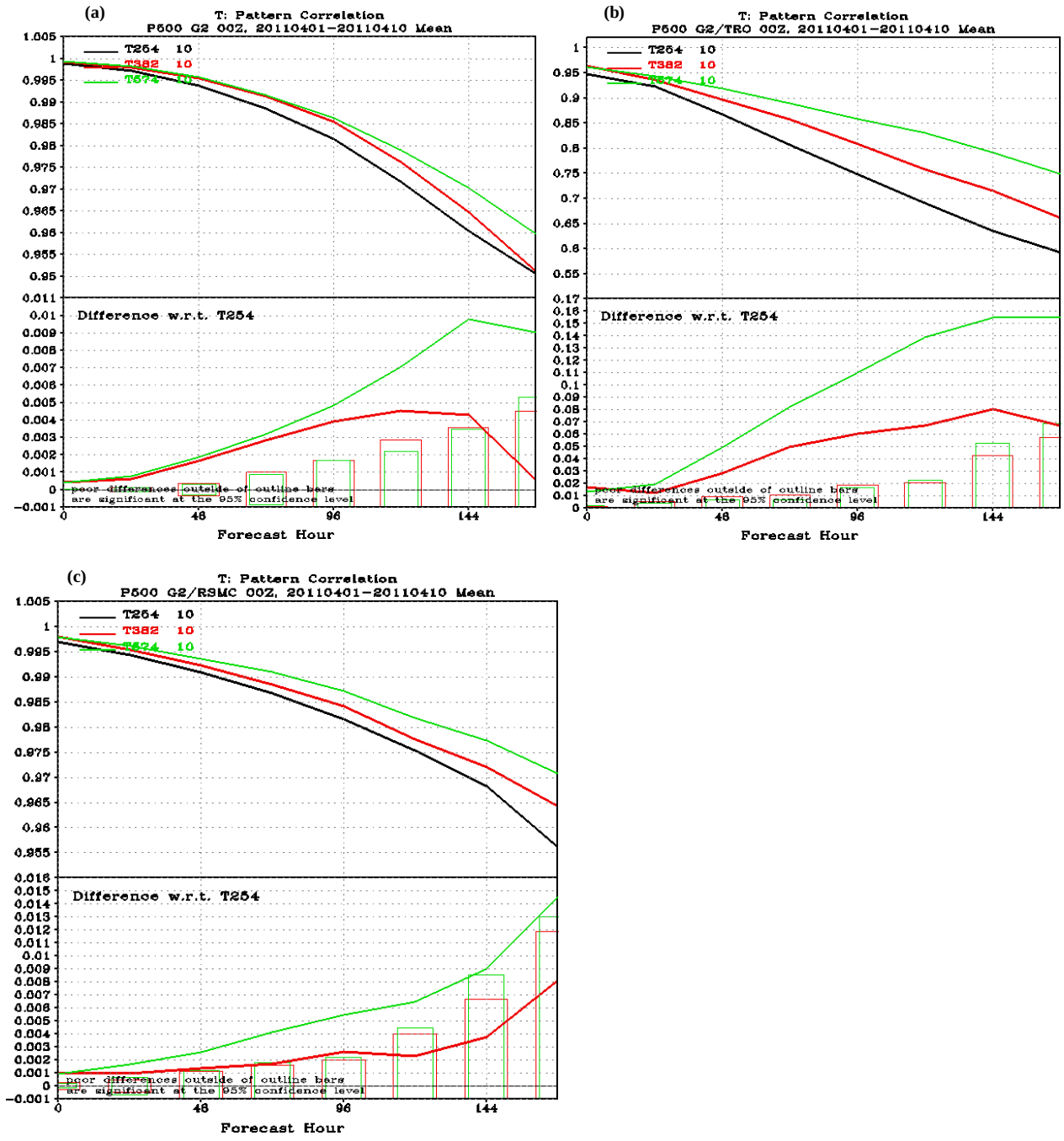

Figure 29: Temperature Pattern Correlation (PC) at 500hPa (upper part) and difference of Mean (PC) w.r.to T254L64 and its statistical significance (lower part) over (a) Globe, (b) Tropics, and (c) RSMC region.

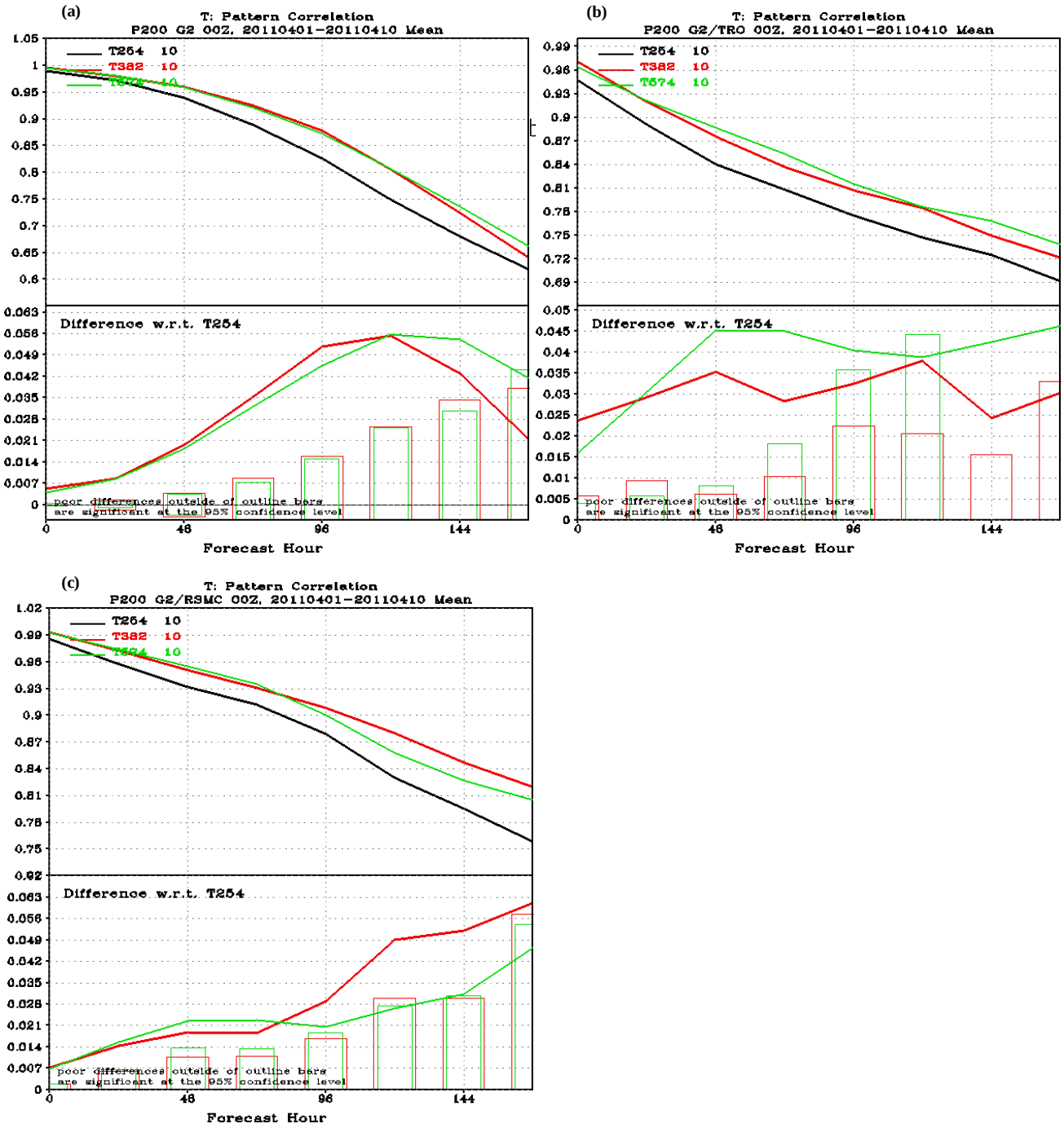

Figure 30: Same as figure 29 but at 200hPa pressure level.

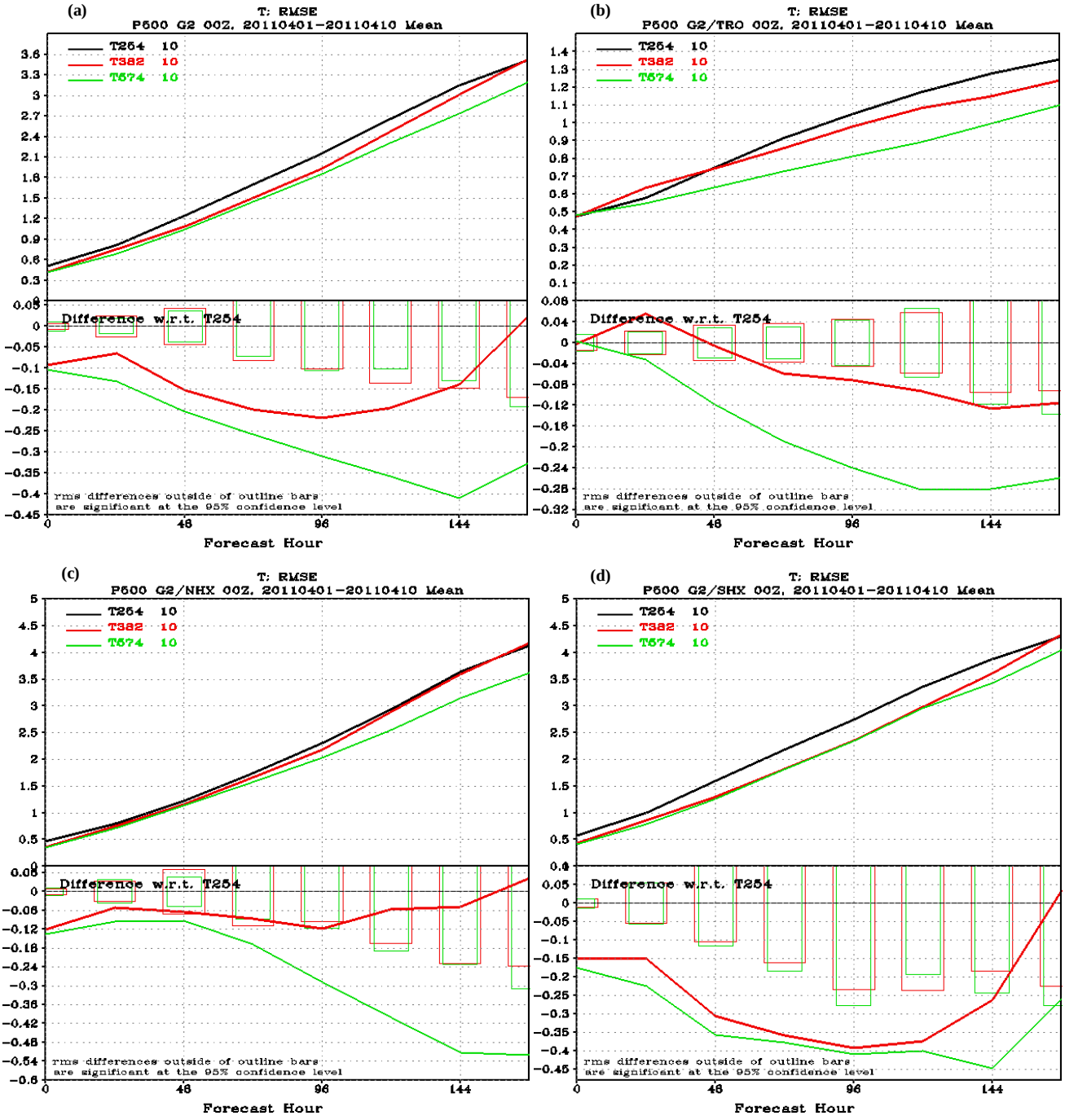

Figure 31: Root Mean Square Error (RMSE) of Temperature at 500hPa (upper part) and difference of Mean (RMSE) w.r.t T254L64 and its statistical significance (lower part) for (a) Globe, (b) Tropics, (c) Northern Hemisphere and (d) Southern Hemisphere.

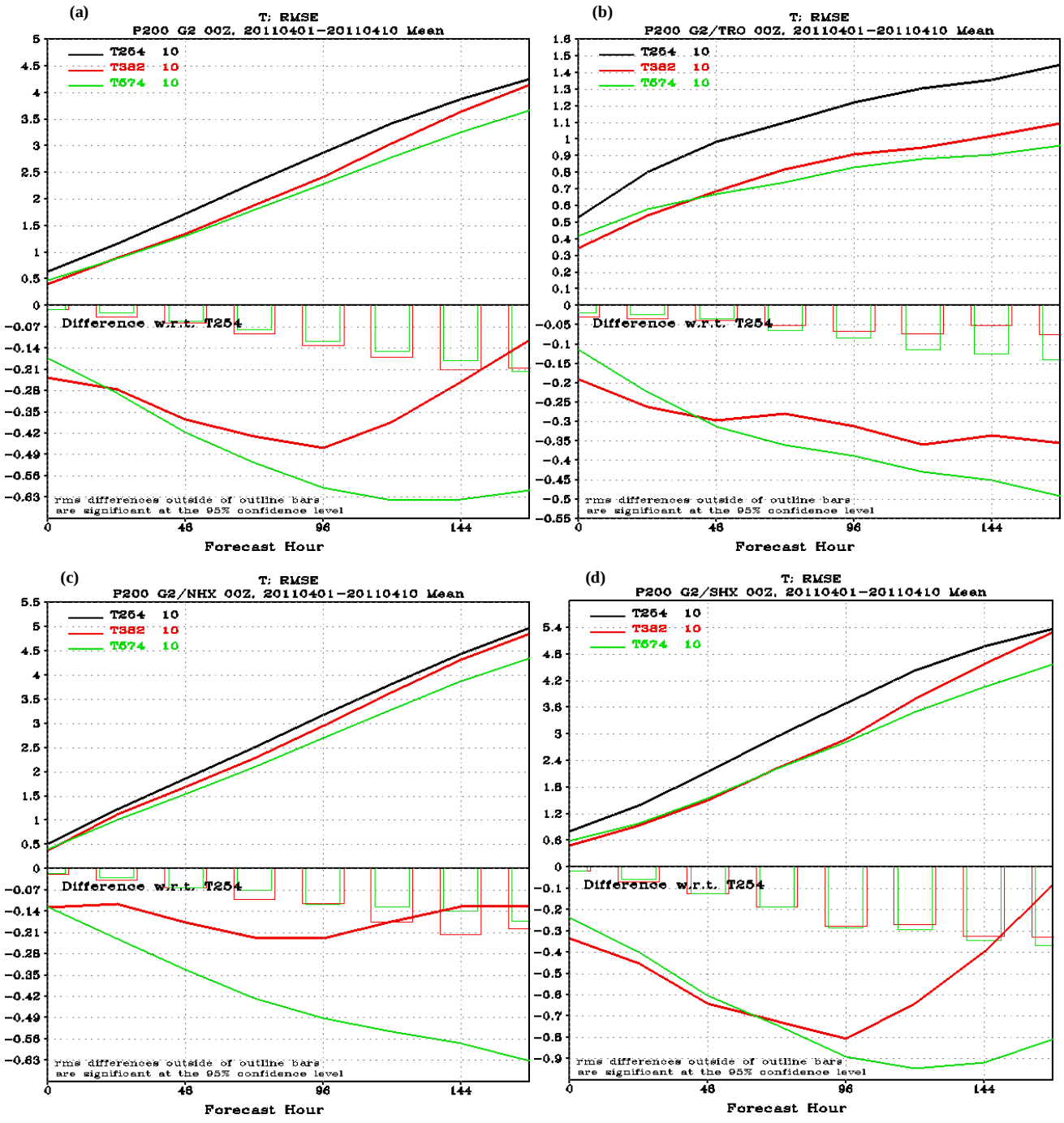

Figure 32: Same as figure 31 but at 200hPa pressure

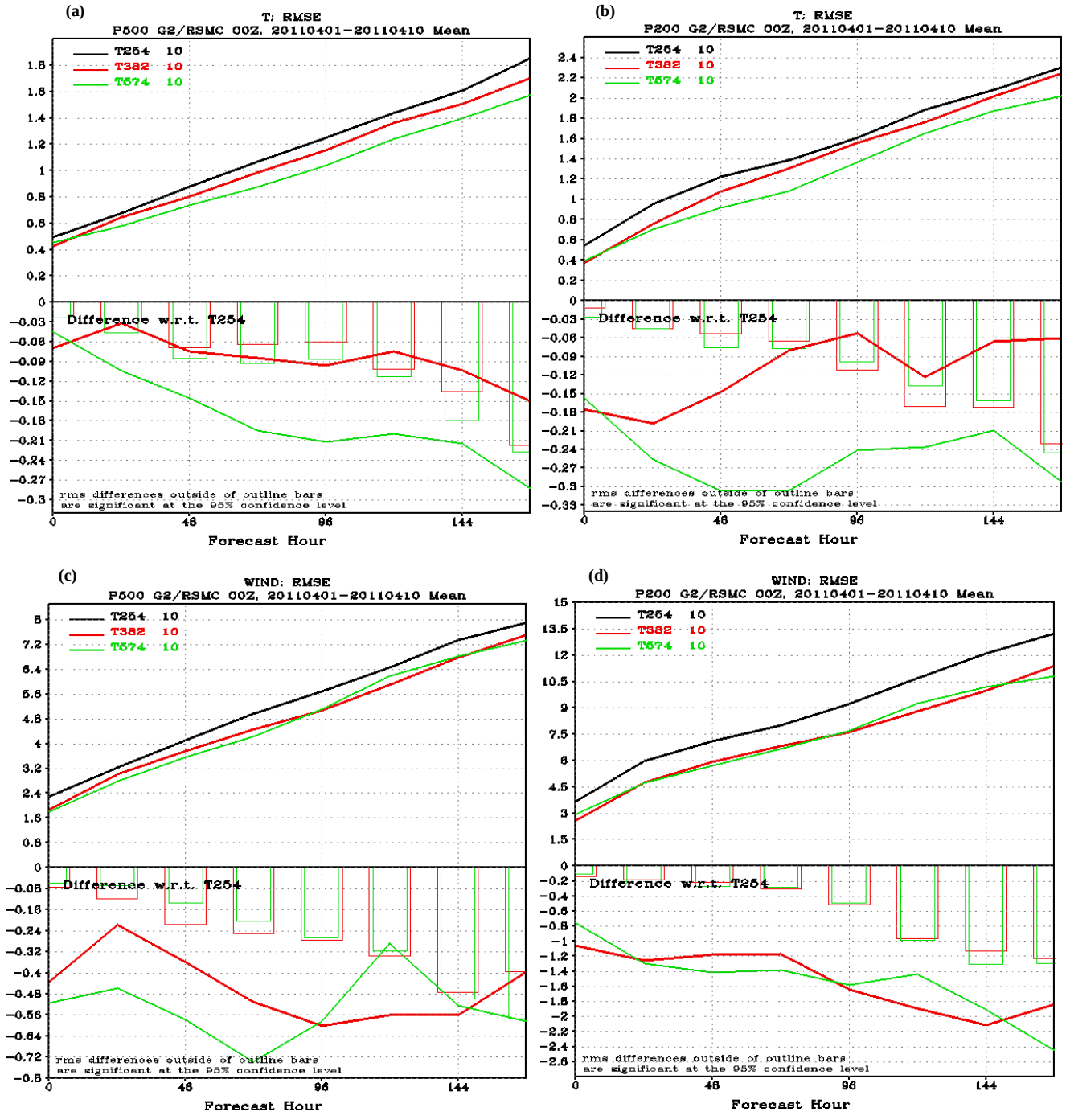

Figure 33: Root Mean Square Error (RMSE) over RSMC region (upper part) and difference of Mean (RMSE) w.r.to T254L64 and its statistical significance (lower part) for Temperature at (a) 500hPa & (b) 200hPa and for Vector Wind at (c) 500hPa & (d) 200hPa.

Acknowledgements

The authors are grateful to NCEP, USA for providing the codes and support for the implementation of the upgrades. (Special thanks to Dr. V Krishnakumar, Dr. Shrinivas Moorthi, Dr. Henry Juang and Dr. Fanglin Yang of NCEP for the useful discussions and personal communications). Thanks are also due to Head, NCMRWF for his constant encouragement and support. The IBM/HCL team is gratefully acknowledged for all the system support provided for the implementation of the libraries and tools in IBM P6 HPC at NCMRWF and the computer division and CMC team for the operational running and implementation of the models.

References

Alpert, J. C., M. Kanamitsu, P. M. Caplan, J.G. Sela, G. H. White, and E. Kalnay, 1988: Mountain induced gravity wave drag parameterization in the NMC medium-range forecast model. *Proc. 8th Conf. on NWP*, Baltimore, MD.

Alpert, J. C., S.-Y. Hong, and Y.-J. Kim, 1996: Sensitivity of cyclogenesis to lower tropospheric enhancement of gravity wave drag using the environmental modeling center medium range model. *Proc. 11th Conf. on NWP*, Norfolk, VA.

Asselin, R., 1972: Frequency filter for time integrations. Mon. Wea. Rev., 100, 487–490.

Clough, S.A., M.W. Shephard, E.J. Mlawer, J.S. Delamere, M.J. Iacono, K. Cady-Pereira, S. Boukabara, and P.D. Brown, 2005: Atmospheric radiative transfer modeling: a summary of the AER codes, *J. Quant., Spectrosc. Radiat. Transfer*, **91**, 233-244.

Charnock, H., 1955: Wind stress on a water surface. Quart. J. Roy. Meteor. Soc., 81, 639-640.

Courtier, P., and Coauthors, 1998: The ECMWF implementation of the three-dimensional variational assimilation (3D-Var). I: Formulation, *Quarterly Journal of Royal Meteorological Society*, 124, pp. 1783-1807.

Cucurull, L., J. Derber, R. Treadon, and R. Purser, 2007: Assimilation of global positioning system radio occultation observations into NCEP's global data assimilation system. *Mon. Wea. Rev.*, 135, 3174–3193.

Derber, J.C., and W.-S Wu, 1998: The use of TOVS cloud-cleared radiances in the NCEP SSI analysis system. *Mon. Wea. Rev*., 126, 2287-2299.

Ek M.B., K.E. Mitchell, Y. Lin, E. Rogers, P. Grunmann, V. Koren, G. Gayno, and J.D. Tarplay, 2003: Implementation of the Noah land-use model advances in the NCEP operational mesoscale Eta model. *J. Geophys. Res.*, **108**, 8851, doi:10.1029/2002JD003296.

Environmental Modeling Centre, 2003: The GFS Atmospheric Model, *NCEP Office Note 442*, 12pp.

Han, J. and H.-L. Pan, 2006: Sensitivity of hurricane intensity forecast to convective momentum transport parameterisation, *Mon. Wea. Rev*., 134, 664-674.

Han, J. and H.-L. Pan, 2010: Revision of Convection and Vertical Diffusion Schemes in the NCEP Global Forecast System, *NCEP Office Note 464*, 42pp. [Available online at: http://www.emc.ncep.noaa.gov/officenotes/newernotes/on464.pdf]

Hong, S.-Y., 1999: New global orography data sets. *NCEP Office Note #424*. [Available online at: http://www.ncep.noaa.gov/officenotes/NOAA-NPM-NCEPON-0006/01408B67.pdf]

Hong, S. -Y. and H. -L. Pan, 1996: Nonlocal boundary layer vertical diffusion in a medium range forecast model. *Mon. Wea. Rev.*, **124**, 2322-2339.

Hong, S. -Y. and H. -L. Pan, 1998: Convective Trigger Function for a Mass-Flux Cumulus Parameterization Scheme. *Mon. Wea. Rev*., **126**, 2599–2620.

Hu, Zing-Zhen, Bohua Huang, and Kathy Degion, 2008: Low cloud errors over the southern Atlantic in the NCEP CFS and their association with lower-tropospheric stability and air-sea interaction, *JGR*, 113:D12114, doi:10.1029/2007JD009514.

Hu, Zing-Zhen, Bohua Huang, Yu-Tai Hou, Wangiu Wang, Fanglin Yang, Cristiana San and Edwin K Schneider, 2010: Sensitivity of tropical climate to low-level clouds in the NCEP climate forecast system, *Clim. Dyn*., doi:10.1007/s00382-010-0797-2.

Iacono, M.J., E.J. Mlawer, S.A. Clough, and J.-J. Morcrette, 2000: Impact of an improved longwave radiation model, RRTM, on the energy budget and thermodynamic properties of the NCAR Community Climate Model, CCM3, *J. Geophys. Res*., **105**, 14873-14890, 2000.

Janji´c, Z., 1990: The step-mountain coordinate physical package. *Mon. Wea. Rev*., 118, 1429–1443.

Kalnay, M. Kanamitsu, and W.E. Baker, 1990: Global numerical weather prediction at the National Meteorological Centre, *Bull. Amer. Meteor. Soc*., 71, 1410-1428.

Kanamitsu, M., 1989: Description of the NMC global data assimilation and forecast system, *Wea. Forecasting*, 4, 335-342.

Kanamitsu, M., J.C. Alpert, K.A. Campana, P.M. Caplan, D.G. Deaven, M. Iredell, B. Katz, H.-L. Pan, J. Sela, and G.H. White, 1991: Recent changes implemented into the global forecast system at NMC, *Wea. Forecasting*, 6, 425-435.

Kessler, E., 1969: On the distribution and continuity of water substance in atmospheric circulation, *Meteorological Monographs*, 10, 84pp.

Kim, Y.-J., A. Arakawa, 1995: Improvement of Orographic Gravity Wave Parameterization Using a Mesoscale Gravity Wave Model. *J. Atmos. Sci.*, **52**, 1875–1902.

Kleist, Daryl T., David F. Parrish, John C. Derber, Russ Treadon, Ronald M. Errico and Runhua Yang, 2009: Improving Incremental Balance in the GSI 3DVAR Analysis System, *Mon. Wea. Rev.*, 137, 1046-1060.

Le Marshall, J. and co–authors, 2001: Improving global analysis and forecasting with AIRS. *Bull. Amer. Meteor. Soc.*, 87, 891–894.

Mellor, G. L. and T. Yamada, 1974: A hierarchy of turbulence closure models for planetary boundary layers, *J. Atmos. Sci.*, 31, 1791–1806.

Miyakoda, K., and J. Sirutis, 1986: Manual of the E-physics. [Available from Geophysical Fluid Dynamics Laboratory, Princeton University, P.O. Box 308, Princeton, NJ 08542.]

Mlawer E. J., S. J. Taubman, P. D. Brown, M.J. Iacono and S.A. Clough, 1997: radiative transfer for inhomogeneous atmosphere: RRTM, a validated correlated-K model for the longwave. *J. Geophys. Res.*, **102**(D14), 16, 663-16, 6832.

Moorthi, S., H. L. Pan and P. Caplan, 2001: Changes to the 2001 NCEP operational MRF/AVN global analysis/forecast system. *NWS Technical Procedures Bulletin*, 484, pp14. Available at http://www.nws.noaa.gov/om/tpb/484.htm.

Okamoto, K. and J. C. Derber, 2006: Assimilation of SSM/I radiances in the NCEP global data assimilation system. *Mon. Wea. Rev.*, 134, 2612–2631.

Pan, H.-L. and W.-S. Wu, 1995: Implementing a mass flux convective parameterization package for the NMC medium range forecast model. *NMC Office Note 409*, 40 pp.[Available online at: http://www.emc.ncep.noaa.gov/officenotes/FullTOC.html#1990]

Parrish, D. F., and J. C. Derber, 1992: The National Meteorological Center's Spectral Statistical-Interpolation Analysis System, *Mon. Wea. Rev.*, 120, 1747-1763.

Rajagopal, E.N., Munmun Das Gupta, Saji Mohandas, V.S. Prasad, Jhon P. George, G. R. Iyengar and D. Preveen Kumar, 2007: Implementation of T254L64 Global Forecast System at NCMRWF, *NCMRWF Technical Report*, pp. 1-42.

Rajagopal, E. N., Surya Kanti Dutta, V. S. Prasad, G. R. Iyenger and M. Das Gupta, 2008:

'Impact of Gridpoint Statistical Interpolation Scheme over Indian Region', *Extended Abstracts: International Conference on Progress in Weather and Climate Modeling Over Indian Region*, 9-12 December, 2008, NCMRWF, pp. 202-205.

Sela, J., 2009, Implementation of the sigma pressure hybrid coordinate into GFS, *NCEP Office Note # 461* [Available at http://www.emc.ncep.noaa.gov/officenotes/FullTOC.html#2000].

Sundqvist, H., E. Berge, and J. E. Kristjansson, 1989: Condensation and cloud studies with mesoscale numerical weather prediction model. *Mon. Wea. Rev.*, **117**, 1641-1757.

Winton, M., 2000: A Reformulated Three-Layer Sea Ice Model. *J. Atmos. Oceanic Technol.*, **17**, 525–531.

Wood, Robert, Christopher S. Bretherton, 2006: On the relationship between stratiform low cloud cover and lower-Tropospheric stability, *J. Climate*, 19, 6425-6432.

Wu, W.-S, R. J. Purser, and D. F. Parrish, 2002: Three-Dimensional Variational Analysis with Spatially Inhomogenous Covariances, *Mon. Wea. Rev*., December, vol. 130, pp. 2905-2916.

Wu, X., K. S. Moorthi, K. Okomoto, and H. L. Pan, 2005: Sea ice impacts on GFS forecasts at high latitudes. *Proceedings of the 85th AMS Annual Meeting, 8th Conference on Polar Meteorology and Oceanography*, San Diego, CA.

Xu, K.-M., and D.A. Randall, 1996: A semiempirical cloudiness parameterisation for use in climate models, *J. Atmos. Sci*., 53, 3084-3102.

Lock, A.P, A.R. Brown, M.R. Bush, G.M. Martin, and R.N.B. Smith, 2000: A new boundary layer mixing scheme. Part-I: Scheme description and single column model tests, *Mon. Wea. Rev*., 128, 3187-3199.

Yang, F., K. Mitchell, Y.-T. Hou, Y. Dai, X. Deng, Z. Wang, and X.-Z. Liang, 2008: Dependence of land surface albedo on solar zenith angle: Observations and model parameterisations, *J. Climate Appl. Meteor*., 47, 2963-2982.

Yang, F, et al., 2009: On the negative water vapor in the NCEP GFS; Sources and Solutions, *23rd Conference in Weather Analysis and Forecasting/19th Conference on Numerical Wether Prediction*, Amer. Meteor. Society, 1-5 June, 2009, Omaha, NE.

Zhao, Q. Y., and F. H. Carr, 1997: A prognostic cloud scheme for operational NWP models. *Mon. Wea. Rev.*, **125**, 1931-1953.